

Journal of Sedimentary Research, 2024, v. 94, 641–662 Research Article

DOI: 10.2110/jsr.2024.004



AGE AND PROVENANCE RELATIONSHIPS BETWEEN THE BASAL GREAT VALLEY GROUP AND ITS UNDERLYING BASEMENT: IMPLICATIONS FOR INITIATION OF THE GREAT VALLEY FOREARC BASIN, CALIFORNIA, U.S.A.

MARIAH C. ROMERO, DEVON A. ORME, KATHLEEN D. SURPLESS, CHANCE B. RONEMUS, *1 AND ZACHARY MORROW Department of Earth Sciences, Montana State University, P.O. Box 173480, Bozeman, Montana 59717, U.S.A.

*2Department of Geosciences, Trinity University, One Trinity Place, #45, San Antonio, Texas 78212, U.S.A.

*e-mail: devon.orme@montana.edu

The Great Valley forearc (GVf) basin, California, records deposition along the western margin of North America during active oceanic subduction from Jurassic through Paleogene time. Along the western GVf, its underlying basement, the Coast Range Ophiolite (CRO), is exposed as a narrow outcrop belt. CRO segments are overlain by the Great Valley Group (GVG), and locally, an ophiolitic breccia separates the CRO from basal GVG strata. New stratigraphic, petrographic, and geochronologic data (3865 detrital and 68 igneous zircon U-Pb ages) from the upper CRO, ophiolitic breccia, and basal GVG strata clarify temporal relationships among the three units, constrain maximum depositional ages (MDAs), and identify provenance signatures of the ophiolitic breccia and basal GVG strata. Gabbroic rocks from the upper CRO yield zircon U-Pb ages of 168.0 ± 1.3 Ma and 165.1 ± 1.2 Ma. Prominent detrital-zircon age populations of the ophiolitic breccia and GVG strata comprise Jurassic and Jurassic-Early Cretaceous ages, respectively, with pre-Mesozoic ages in both that are consistent with sources of North America affinity. Combined with petrographic modal analyses that show abundant volcanic grains (> 50%), we interpret the breccia to be mainly derived from the underlying CRO, with limited input from the hinterland of North America, and the basal GVG to be derived from Mesozoic igneous and volcanic rocks of the Sierra Nevada-Klamath magmatic arc and hinterland. Analysis of detrital-zircon grains from the lower and upper ophiolitic breccia yields MDAs of \sim 166 Ma and \sim 151 Ma, respectively. Along-strike variation in Jurassic and Cretaceous MDAs from basal GVG strata range from \sim 148 to 141 Ma, which are interpreted to reflect diachronous deposition in segmented depocenters during early development of the forearc. The ophiolitic breccia was deposited in a forearc position proximal to North America < 4 Myr before the onset of GVG deposition. A new tectonic model for early development of the GVf highlights the role of forearc extension coeval with magmatic arc compression during the earliest stages of basin development.

INTRODUCTION

Forearc basins evolve oceanward of active volcanic arcs, making them important sediment archives that record the erosional history of the upper plate and changes in subduction zone dynamics in convergent margins (e.g., Dickinson 1995; Clift and Vannucchi 2004). The Great Valley forearc (GVf) basin, California (Fig. 1) preserves an > 100 million-year sedimentary record from Mesozoic to Cenozoic time (e.g., Goudkoff 1945; Hackel 1966; Morrison et al. 1971; Ingersoll 1976, 1978; Dickinson and Seely 1979; Graham 1981; Almgren and Hacker 1984; Moxon 1988; Williams 1997). The GVf evolved above accretionary and continental-arc crust along its central to eastern margin and trapped oceanic crust along its western margin (Cady 1975; Ingersoll 1982; Godfrey et al. 1997; Constenius et al. 2000; Williams and Graham 2013; Orme and Graham 2018). Good preservation of the GVf basin, relative to other ancient forearc systems that have been eroded and deformed (e.g., Dickinson

1995; Ingersoll 2012; Orme et al. 2021), allow thorough study of how forearc systems may evolve across different basement terranes.

Pioneering investigations of the Great Valley Group (GVG), Mesozoic strata that constitute much of the basin, shed light on Jurassic-Paleogene arc-forearc development and configuration using sandstone petrofacies (e.g., Ojakangas 1968; Dickinson and Rich 1972; Ingersoll 1983), conglomerate clast compositions (e.g., Bertucci 1983; Seiders and Blome 1988), and paleocurrent analysis (e.g., Ojakangas 1968; Ingersoll 1979; Suchecki 1984). Subsequent geochronologic analyses further detailed links between the basin and its magmatic source regions in the Sierra Nevada-Klamath arcs and continental interior (e.g., DeGraaff-Surpless et al. 2002; Sharman et al. 2015; Orme and Surpless 2019; Surpless et al. 2019). In addition, subsurface and outcrop studies document eastward widening of the basin through time, with the youngest strata onlapping the Sierra Nevada foothills, including the westernmost part of the Cretaceous magmatic arc (e.g., Ingersoll 1982; Constenius et al. 2000; Mitchell et al. 2010; Williams and Graham 2013; Orme and Graham 2018). Decades of studies have significantly contributed to understanding GVf basin evolution, but the age of the basal GVG stratigraphy and its tectonic

Published Online: October 2024

Copyright © 2024, SEPM (Society for Sedimentary Geology) 1527-1404/24/094-641

^{*} Present Address: Department of Geosciences, University of Arizona, Tucson, Arizona 85721, U.S.A.

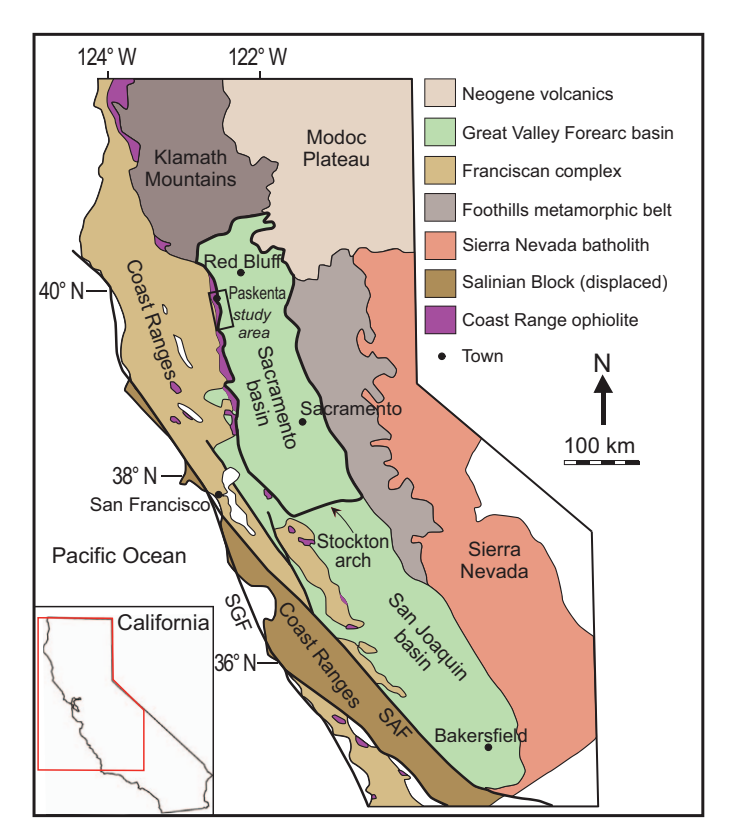


Fig. 1.—Generalized geologic map of northern California. Black rectangle near Paskenta outlines study area, in which sections were measured in basal strata of the Great Valley forearc (GVf) basin (green). Sacramento basin is outlined by bold black line. SAF, San Andreas fault; SGF, San Gregorio fault. Modified from Orme and Graham (2018).

setting during initial deposition are still debated (e.g., Ingersoll 2019; Orme and Surpless 2019; Zakharov and Rogov 2020).

Along the northwestern margin of the Sacramento basin (Fig. 1), segments of the Middle to Late Jurassic Coast Range Ophiolite (CRO) basement are exposed in a narrow outcrop belt, where they are overlain by basal GVG strata; locally, ophiolitic breccia separates the CRO from GVG strata. The origins of the CRO are debated (e.g., Saleeby 1982, 1992; Shervais 2001; Shervais et al. 2005, and references therein; Hopson et al. 2008, and references therein; Ingersoll 2019, and references therein), as well as the mechanism driving the development of the sedimentary breccia that locally overlies the CRO; it remains unclear whether the breccia was deposited proximal or distal to the North American margin in the Late Jurassic (e.g., Lagabrielle et al. 1986; Robertson 1990; Hopson et al. 2008). This uncertainty limits our understanding of the age and tectonic relationship between basal GVG stratigraphy and its underlying basement during development of the North America Cordillera and how continentalmargin forearc basins evolve atop oceanic basement. For example, hypotheses for the formation of forearc basins center around the role of the accretionary prism and orogenic wedge, including changes in sediment flux and geometry at the plate boundary (e.g., Dickinson and Seely 1979; Noda 2016) and the response of the upper plate to changes in the critical taper of the deforming wedge (Fuller et al. 2006; Willett and Schlunegger 2010). However, few studies have investigated the role, if any, the rocks underlying the basin may play in driving development of accommodation (e.g., Maffione et al. 2015). This study reports new stratigraphic, petrographic, and geochronologic data from the northern Sacramento basin to re-evaluate the age and provenance of the basal GVG and its

	Ö			STRATIO	GRAPHY	
STAGE (Ma)	PERIOD	AGE	Ingersoll (1983)	Surpless et al. (2006)	Orme and Surpless (2019)	This Study NW Sacramento basin
_100 _		Cenomanian				
-110-	C R E T	Albian	Lodoga Fm.	Lodoga Fm.	Lodoga Fm.	Lodoga Fm.
-120-	A C	Aptian				
-130-	E O U	Barremian Hauterivian	Platina Fm.	Platina Fm.	Platina Fm.	Stony Creek Fm.
140	S	Valanginian Berriasian	Stony Creek Fm.	Stony Creek Fm.		
_150 _	J U R	Tithonian				
	Α	Kimmeridgian	Coast	Coast		cia
_160 _	SS	Oxfordian	Range Ophiolite	Range Ophiolite		ophiolitic breccia
	Ċ	Callovian Bathonian			Coast Range Ophiolite	Coast Range Ophiolite

Fig. 2.—General stratigraphic chart of Upper Jurassic–Lower Cretaceous basement and sedimentary units in the northwestern Sacramento basin. U-Pb analyses of igneous zircon from two sampled plutonic rocks in Coast Range ophiolite (CRO) of this study yield weighted mean ages of 167.02 ± 0.29 Ma (sample 0619-MR-06) and 165.79 ± 0.27 Ma (sample 0619-MR-07). Modified from Surpless et al. (2006).

relationship with underlying basement and breccia. Integrating these data with those of previous studies, we present a tectonic model for the early stages of GVf basin development that proposes extension in the forearc region of the North American convergent margin during Late Jurassic–Early Cretaceous time.

GEOLOGIC BACKGROUND

Geologic Setting

From west to east, the Franciscan Complex, CRO, GVG, and Sierra Nevada magmatic-arc complex record late Mesozoic–Miocene convergence along the western margin of North America (Fig. 1) (e.g., Hamilton 1969; Engebretson et al. 1985). The Franciscan accretionary complex is an assemblage of low- and high-grade metamorphic and sedimentary rocks deposited in or near a trench and accreted in a subduction zone (Ernst 1970; Wakabayashi 2011). Structurally overlying the Franciscan Complex, the CRO represents the oceanic basement of the western GVf basin (Bailey et al. 1970; Ingersoll 1982); igneous and metamorphic rocks of the Sierra Nevada foothills form the basement along the eastern basin margin (Cady 1975; Godfrey et al. 1997; Schweickert 2015; Orme and Graham 2018). The Coast Range thrust marks the contact between the Franciscan Complex and the CRO; the GVG is in both tectonic and depositional contact with the CRO (Ingersoll 1982, 2019; Dickinson 1995).

The age of upper CRO varies from ~ 174 to 164 Ma throughout the northern Sacramento basin (Fig. 2). Zircon U-Pb ages for the Elder Creek and Stonyford segments of the ophiolite are 172–165 Ma and 172–166 Ma, respectively (Shervais et al. 2005). In our study area, the CRO in Grindstone Creek yields a titanite U-Pb age of ~ 167 Ma (Orme and Surpless 2019) and, immediately west of Paskenta, a hornblende K-Ar age of ~ 163 Ma (Fritz 1975). Radiolarian assemblages from cherts interbedded with CRO volcanics in the Stonyford area range in age from Bathonian at the base to early Kimmeridgian at the top of the succession

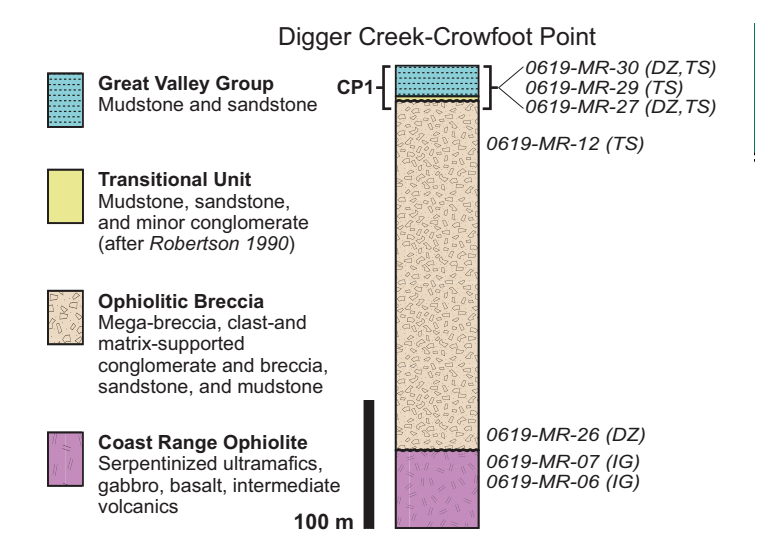


Fig. 3.—Stratigraphic column for Coast Range ophiolite and overlying sedimentary successions for Digger Creek area, north of Crowfoot Point. Modified after Robertson (1990), following field observations in this study. Sample abbreviations: DZ, detrital-zircon sample for U-Pb analyses; IG, igneous-zircon sample for U-Pb analyses; TS, thin section.

(Shervais et al. 2005, and references therein). Proposed models for development of the CRO include: 1) backarc–interarc spreading behind an east-facing intra-oceanic island arc that was subsequently accreted to the Sierra Nevada arc via arc collision during Jurassic time (Ingersoll 2019, and references therein), 2) mid-ocean ridge spreading in an openocean setting, at or near paleoequatorial latitude; this mobile oceanic crust was then transported northward to a position outboard of the Sierra Nevada continental-margin arc (Dickinson et al. 1996; Hopson et al. 2008, and references therein), or 3) forearc spreading in response to slab rollback in the forearc region of the Sierra Nevada continental-margin arc during the end of Middle Jurassic time (Shervais et al. 2005, and references therein). Most recently, Orme and Surpless (2019) invoked the latter model to help explain diachronous depositional ages in the earliest forearc.

Coast Range Ophiolitic Breccia

Stratigraphy.—In northern California, several remnants of the CRO are overlain by sedimentary ophiolitic breccia and a thin transitional unit of mudstone beneath deep-water facies assigned to the GVG (Figs. 3, 4) (Bezore 1969; Bailey et al. 1970; Bailey and Blake 1974; Evarts 1977; Hopson et al. 1981; Lagabrielle et al. 1986; Blake et al. 1987; McLaughlin et al. 1988; Robertson 1990). The ophiolitic breccia outcrops along $\sim 9 \text{ km}$ of the CRO-GVG contact, and is mapped as part of the CRO; its stratigraphic thickness varies along strike and ranges from ~ 1 m to ~ 600 m (Hopson et al. 1981; Lagabrielle et al. 1986; Robertson 1990). The unit consists of mega-breccia, clast-supported breccia, clast- and matrixsupported conglomerate, sandstone, and mudstone (Lagabrielle et al. 1986; Robertson 1990). Clasts in the ophiolitic breccia include basalt, gabbro, plagiogranite, anorthosite, pyroxenite, fine-grained mafic dike rocks, diabase, and radiolarian chert (Hopson et al. 1981, 2008; Lagabrielle et al. 1986; Robertson 1990). The age of the ophiolitic breccia is interpreted as Late Jurassic (Kimmeridgian), based on preservation of Buchia rugosa at Crowfoot Point, in the Paskenta area (Jones 1975; Pessagno 1977).

At Digger Creek, near Crowfoot Point, Robertson (1990) described a "transitional unit" containing lower Tithonian radiolarians, and consisting of siliceous mudstone, sandstone, and minor conglomerate between the

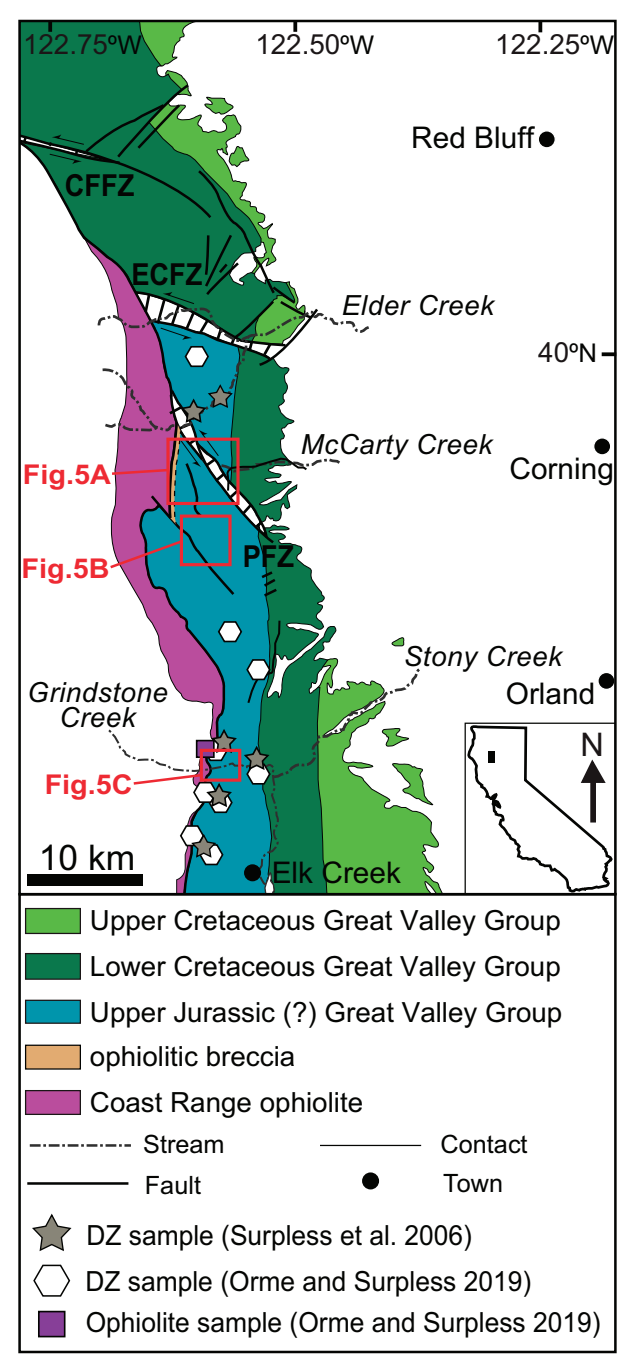


Fig. 4.—Generalized geologic map showing sample locations from previous studies in northwestern Sacramento basin. Red boxes indicate sample location maps (Fig. 5A–C) for this study. White, striped pattern represents fault zones. CFFZ, Cold Fork fault zone; ECFZ, Elder Creek fault zone; PFZ, Paskenta fault zone. Modified from Orme and Surpless (2019).

underlying ophiolitic breccia and the overlying GVG (Fig. 3). North of Digger Creek, near Elder Creek, the CRO (referred to as Elder Creek ophiolite remnant in Hopson et al. 2008) is overlain by > 4 m of reddish-brown tuffaceous radiolarian chert, ophiolitic breccia, and thin volcanopelagic beds that are referred to as the "transitional unit" by Robertson (1990). In contrast, Hopson et al. (2008) reported this CRO remnant as overlain by sedimentary

ophiolitic breccia that was syndepositional with basal GVG. Approximately 2 km north and at the head of Digger Creek, Lagabrielle et al. (1986) reported a basaltic sill that cuts across ophiolitic breccia and basal GVG mudstone, interpreting this to reflect a Late Jurassic magmatic event. Together, these observations suggest spatially variable stratigraphic relations along the western side of the Sacramento basin, warranting additional study of the temporal relationships among the CRO, ophiolitic breccia, and GVG.

Provenance and Tectonic Setting.—The ophiolitic breccia contains debris from various levels of the underlying ophiolite and has been interpreted to represent dismemberment of the underlying oceanic crust (e.g., Hopson et al. 1981, 2008; Lagabrielle et al. 1986; Blake et al. 1987; Robertson 1990). Robertson (1990) suggested that the transitional unit contains magmatic-arc-derived detritus, based on the presence of subordinate silicic volcanic and tuffaceous sediment. Hopson et al. (2008) suggested that the interstratified siliceous sediment and tuff beds in the transitional unit of Robertson (1990) represent the upper volcanopelagic succession of the CRO oceanic crust, but interpreted the ophiolitic sandstone debris as reworked from the underlying ophiolitic breccia

Numerous mechanisms have been proposed to produce the ophiolitic breccia. Lagabrielle et al. (1986) suggested that faulting and erosion of the CRO occurred before or during deposition of the breccia in an island-arc and extensional back-arc environment, based on trace-element analysis. Robertson (1990) suggested that extensional faulting resulted in rock fall and slumping, along with sliding, debris-flow, turbidity, and tractioncurrent deposition to deposit the ophiolitic breccia and transitional unit. In contrast, Hopson et al. (2008) argued that faulting and the production of bedrock fault scarps cannot explain the voluminous fragmental debris that extended over large areas of the seafloor during Late Jurassic time. They proposed that dismembered oceanic crust developed large structural relief via faulting that occurred before, during, and after breccia deposition. Hopson et al. (2008) further proposed that crustal fault slices, extensive fragmental ophiolitic debris, and finer sediments were produced in a migrating transform zone located between a propagating rift tip and the failing rift in a deep-sea setting during Late Jurassic distal volcanopelagic sedimentation. In addition, the Late Jurassic collision between island-arc terranes and North America, termed the Nevadan orogeny (e.g., Knopf 1929; Schweickert et al. 1984), may have contributed to creation of the breccia (Ingersoll 1982, 2019; Schweickert 2015). Ingersoll (1982) interpreted ophiolitic detritus in the basal GVG as evidence for erosion of "tectonic highlands" of the CRO formed during the arc-arc collision of the Nevadan orogeny.

Great Valley Group

Stratigraphy and Depositional Age.—The Sacramento basin is separated from the San Joaquin basin by the Cenozoic Stockton arch (Fig. 1). The Mesozoic GVG is preserved as an eastward-dipping homoclinal belt along the western side of the Sacramento basin (Kirby 1943; Ingersoll et al. 1977). The basal GVG in the Sacramento basin is the Stony Creek Formation, which rests unconformably on the upper CRO, or locally the ophiolitic breccia (Figs. 2, 3). The basal GVG strata record a lithologic shift from Tithonian(?)—Berriasian ophiolitic, volcaniclastic sandstone and pelagic sediment that overlie the CRO to Valanginian—Albian mudstone, sandstone, and conglomerate (Ingersoll 1982; Robertson 1990). This study uses "Tithonian(?)" and "Upper Jurassic(?)" to indicate the uncertainty of the Jurassic age assignment (Surpless et al. 2006; Orme and Surpless 2019; Zakharov and Rogov 2020).

Recent work by Zakharov and Rogov (2020) on the nomenclature and biostratigraphic zonal boundaries at Jurassic-Cretaceous transitional intervals in the Paskenta area of northern California (Figs. 1, 5) suggests that buchild bivalves and ammonites from McCarty

Creek and Grindstone Creek (Figs. 4, 5) indicate a Tithonian (Late Jurassic) basal age of the GVG. However, Surpless et al. (2006) and Orme and Surpless (2019) documented the presence of Cretaceous detrital zircon in this same stratigraphic interval, suggesting that the chronostratigraphy of basal forearc strata requires re-evaluation and that forearc-basin sedimentation may have began $\sim 10{\text -}20$ Myr after CRO formation. If initial deposition of the GVG occurred later than previously interpreted from biostratigraphy (Tithonian age), and as young as Valanginian–Hauterivian (Surpless et al. 2006; Orme and Surpless 2019), then sedimentation rates could have been significantly higher than previously interpreted (Orme and Graham 2018).

Orme and Surpless (2019) used the Jurassic-Cretaceous boundary of 145 ± 0.8 Ma from Ogg and Hinnov (2012), which was subsequently updated to 145.7 \pm 0.8 Ma (Ogg et al. 2016). However, Lena et al. (2019) present high-precision U-Pb geochronologic data that support a Jurassic-Cretaceous age boundary of 140.9-140.7 Ma. Wimbledon et al. (2020) propose that the Tithonian-Berriasian boundary is at 140.22 ± 0.14 Ma, based on biostratigraphic and magnetostratigraphic data from various global locations that contain the Jurassic-Cretaceous boundary. Furthermore, in the proposed GTS2020 timescale (Gradstein et al. 2020), Gale et al. (2020) define the base of the Berriasian as 143.1 Ma through cyclostratigraphic extrapolations based on the extent of the stage and spline-fitting. Because the proposed age boundaries of Lena et al. (2019), Wimbledon et al. (2020), and Gradstein et al. (2020) are not formally accepted by the International Commission on Stratigraphy (ICS) or the Geological Society of America, we use the ICS published age of ~ 145.0 Ma for the Jurassic-Cretaceous boundary and the revised Upper Jurassic stage boundaries in the International Chronostratigraphic Chart v 2023/09 (Cohen et al. 2013; updated).

Depositional Environments.—Interbedded siltstone—sandstone, massive mudstone, siltstone, shale, and thin-bedded silty sandstone make up most of the deep-marine strata of the Upper Jurassic(?)—Lower Cretaceous Great Valley Group (Ingersoll 1982, 1990; Suchecki 1984). In our study area, Ojakangas (1968), Ingersoll (1978), and Suchecki (1984) were the first to measure stratigraphic sections and interpret depositional environments. These studies documented that Upper Jurassic Tithonian(?)—Lower Cretaceous Berriasian strata of the Stony Creek Formation consist of thick-bedded sandstone with interbedded mudstone and lenticular (channel-fill) pebble—cobble conglomerate, which were interpreted as submarine slope and canyon deposits (Ingersoll 1978; Suchecki 1984).

Provenance.—Previous sandstone petrography and paleocurrent analysis have provided significant insight into the provenance of the northern GVG (e.g., Ojakangas 1968; Dickinson and Rich 1972; Ingersoll 1979, 1983; Suchecki 1984; Short and Ingersoll 1990). In Tithonian(?) strata of the northern GVG, paleoflow indicators suggest southward flow of turbidity currents (Suchecki 1984) sourced from the north. By contrast, Berriasian strata record westward flow (Suchecki 1984). The regional paleoslope from Late Jurassic(?) to Early Cretaceous time was a southwest-dipping slope that allowed detritus to bypass parts of the forearc basin, with deposition directly in the trench (Ingersoll 1978, 1982).

Sandstone petrographic and paleocurrent analyses and mudrock geochemistry support the interpretation that provenance of the GVG was in the Sierra Nevada and the Klamath Mountains (Fig. 1) (Ingersoll 1979, 1983; Bertucci 1983; Suchecki 1984; Short and Ingersoll 1990; Surpless 2014). In addition, Nd-Sr isotopic analyses of sandstones from Sacramento basin strata document ϵ_{Nd} values ranging from -1.6 to +7 (Linn et al. 1992), consistent with ϵ_{Nd} of sediment sources in the northern Sierran foothills terranes, northern Sierra Nevada batholith, and the Klamath Mountains (e.g., DePaolo 1981).

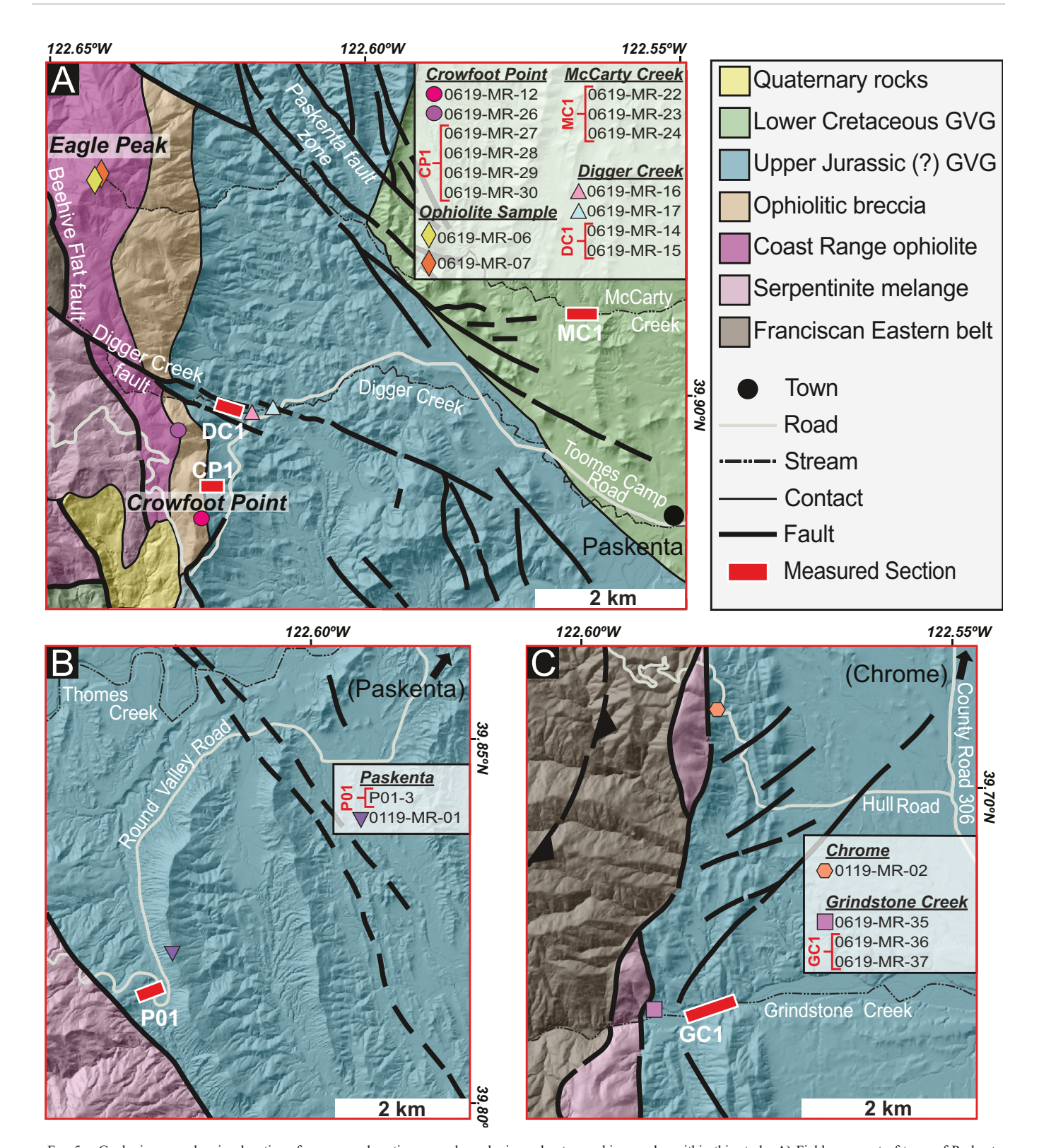


Fig. 5.—Geologic maps showing locations for measured sections, geochronologic, and petrographic samples within this study. A) Field area west of town of Paskenta, including Eagle Peak, Crowfoot Point, McCarty and Digger Creek. B) Field area southwest of Paskenta. C) Field area near Chrome and along Grindstone Creek. Modified from Lagabrielle et al. (1986), Jayko et al. (1987), Robertson (1990), and Blake et al. (1992).

Mesozoic sandstones from the GVG contain prominent Triassic–Early Cretaceous detrital-zircon age modes interpreted to be derived from both the Sierra Nevada and the Klamath Mountains (DeGraaff-Surpless et al. 2002; Surpless et al. 2006; Wright and Wyld 2007; Surpless and Augsburger 2009; Surpless 2014; Martin and Clemens-Knott 2015; Sharman et al. 2015; Greene and Surpless 2017; Orme and Surpless 2019). In addition, the GVG contains pre-Mesozoic zircon interpreted to be derived from Triassic and Paleozoic accreted terranes (e.g., Shoo Fly Complex and Golconda allochthon) and passive-margin strata (e.g., DeGraaff-Surpless et al. 2002). Detrital-zircon age spectra from the GVG record changes in the abundance of pre-Mesozoic age populations interpreted to reflect changes in catchment areas, some of which tapped the interior of the continent (DeGraaff-Surpless 2002; Orme and Surpless 2019).

Paskenta Fault Zone

In the northwestern Sacramento basin, the Cold Fork, Elder Creek, and Paskenta fault zones, which strike approximately northwest–southeast across the Upper Jurassic(?) and Lower Cretaceous GVG (Fig. 4), developed coeval with Jurassic–Cretaceous sedimentation (Jones et al. 1969; Suchecki 1984; Vogel 1985; Moxon 1988, 1990). The Paskenta fault zone is interpreted as a synsedimentary normal fault system (Figs. 4, 5A) (Suchecki 1984; Constenius et al. 2000) with down-to-the-north faulting based on the geometry of seismic reflections, as well as outcrop-scale field relations (Vogel 1985; Vogel and Cloos 1985). Thickening of Tithonian(?)—Turonian GVG strata in the hanging wall of the Paskenta fault zone, as well as the Elder Creek and Cold Fork fault zones to the north (Fig. 4), attenuation or complete omission of the CRO, and subsurface discontinuities in basal GVG strata support syndepositional extension (Constenius et al. 2000).

METHODS

Sedimentology and Stratigraphy

Detailed stratigraphic sections of the basal GVG were measured (cm scale) at five localities using a Jacob's staff to determine depositional environments and provide context for provenance and maximum depositional ages in the northwestern Sacramento basin (Figs. 5, 6, 7). We apply lithofacies codes modified from marine deposits described in Orme et al. (2015, 2021), following the work of Bouma (1962) and Mutti (1992) (Table 1). Fine- to coarse-grained sandstone, along with clast-supported and matrix-supported breccia, were collected for petrologic and U-Pb geochronologic analysis.

Sandstone Modal Analysis

Four thin sections from sandstone collected at the breccia–GVG contact near Crowfoot Point were analyzed to determine their composition and provenance. Additional samples from the GVG were not analyzed owing to prior, detailed petrologic work on the provenance of the GVG (e.g., Dickinson and Rich 1972; Ingersoll 1983; Short and Ingersoll 1990). Sample 0619-MR-27, a very coarse-grained sandstone from the matrix of the upper breccia, and samples 0619-MR-29 and 0619-MR-30, medium-coarse-grained sandstones from the basal GVG, were collected in stratigraphic section CP1 (Fig. 6). Sample 0619-MR-12 is a very coarse-grained sandstone from the matrix of the upper breccia, collected ~ 500 m south of the base of section CP1 (Fig. 5A). The GVG samples were point-counted with at least 300 framework counts per slide, following the Gazzi–Dickinson method of point-counting (Fig. 8) (Gazzi 1966; Ingersoll et al. 1984; Dickinson 1985); the breccia samples had < 75 framework counts per slide due to large grain size and no additional thin sections

available. Photomicrographs of the framework grains and matrix from ophiolitic breccia and basal GVG are shown in Figure 8. Petrographic parameters for modal point-counting are listed and defined in Table 3. Modal data are provided in the Supplemental Material.

Zircon U-Pb Geochronology

Sixteen sandstone samples from the GVG, three samples from the ophiolitic breccia, and two igneous samples from the CRO were collected for U-Pb geochronologic analysis (Table 2). Mineral separation for zircon was completed using standard separation techniques (e.g., Gehrels et al. 2008). Of the 21 samples collected for U-Pb geochronologic analysis, 16 (14 detrital, 2 igneous) yielded enough zircon for dating; analyses were conducted at the Arizona LaserChron Center (Table 2). Probability distribution plots (PDPs) for each detrital-zircon sample were generated using the software package detritalPy (Sharman et al. 2018). Probability distribution plots incorporate analytical uncertainty and visually highlight the youngest age populations due to their higher analytical precision relative to older dates (e.g., Vermeesch 2013). For potential igneous sources, age distributions are shown as histograms because our compilation includes data from laser ablation-inductively coupled plasma-mass spectrometry (LA-ICP-MS) and chemical abrasionisotope dilution-thermally ionized mass spectrometry (CA-ID-TIMS), methods with different analytical precision.

Three hundred and fifteen detrital-zircon grains or 35 igneous grains per sample were randomly selected for analysis, using backscattered electron (BSE) and cathodoluminescence (CL) images of detrital and igneous samples, respectively, to aid in selecting zircon without cracks and/or significant inclusions. All zircon grains were analyzed by LA-ICP-MS using a Thermo Element2 single collector ICP-MS. U-Pb analyses were conducted with a 20 μm spot diameter, resulting in a 12 μm pit depth on each evaluated grain. U-Pb data were filtered to exclude ages with high common Pb, >5% reverse discordance, >10% uncertainty, or >20% discordance. The reported ages are based on the $^{206}\text{Pb}/^{238}\text{U}$ ages for grains $<\sim1.0$ Ga and on the $^{206}\text{Pb}/^{207}\text{Pb}$ ages for grains $>\sim1.0$ Ga (Gehrels et al. 2008; Gehrels 2012). U-Pb data are reported in the Supplemental Material.

The maximum depositional age (MDA) of a detrital sample can be determined from the youngest population of zircon U-Pb ages (e.g., Dickinson and Gehrels 2009). Although MDAs can be significantly older than true depositional age (TDA), detrital-zircon samples from the GVG are likely to yield MDAs that are similar to TDAs due to proximity to the Sierra Nevada-Klamath magmatic arc during the time of deposition (e.g., Orme and Surpless 2019). In addition, our sample size of n = \sim 300 grains for 12 of our 14 samples has been statistically shown to capture all age populations, including the youngest from which we calculate MDAs (e.g., Pullen et al. 2014). This study reports four possible MDAs for 14 detrital-zircon samples: 1) youngest single grain, YSG; 2) youngest contiguous grain cluster of three or more ages with overlapping 2σ uncertainties, YC2 $\sigma(3+)$ (Coutts et al. 2019); 3) the youngest statistical age population with a mean squared weighted deviation (MSWD) of \sim 1.00 (YSP; Coutts et al. 2019; Herriott et al. 2019); and 4) the maximum likelihood age (MLA) (Vermeesch 2021) (Table 4). These MDA metrics were calculated using individual dates at 1 σ error. Before calculating MDAs by the $YC2\sigma(3+)$, YSP, and MLA methods, all samples were screened for young outliers that do not overlap the second youngest grain within 1σ error (e.g., Surpless et al. 2023, resulting in removal of a single outlier grain in each of three samples, 0619-MR-17, 0619-MR-27, and 0619-MR-36. We calculated $YC2\sigma(3+)$ and YSP using DZmda (Sundell et al. 2024) and MLA using IsoplotR (Vermeesch 2018), for which outputs are reported at 2σ uncertainty. In IsoplotR, we accepted a logarithmic transformation and set "finite mixtures" to "minimum" (Vermeesch 2021). For all pooled-age MDAs, a sample-analysis-specific systematic error was

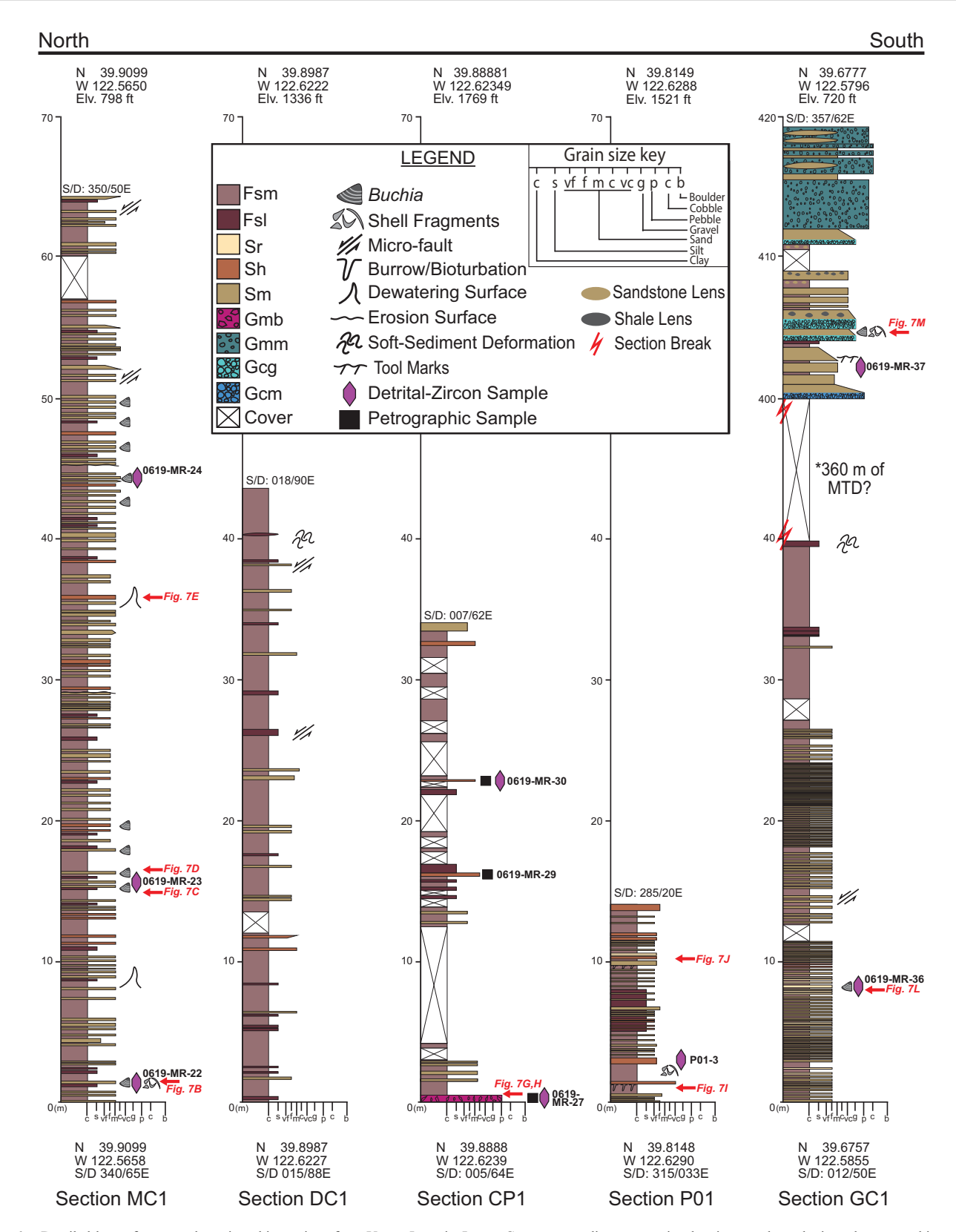


Fig. 6.—Detailed logs of measured stratigraphic sections from Upper Jurassic-Lower Cretaceous sedimentary units showing geochronologic and petrographic samples. Each section was measured using a Jacob staff. Section abbreviations: CP1, Crowfoot Point; DC1, Digger Creek; GC1, Grindstone Creek; MC1, McCarty Creek; P01, Paskenta.

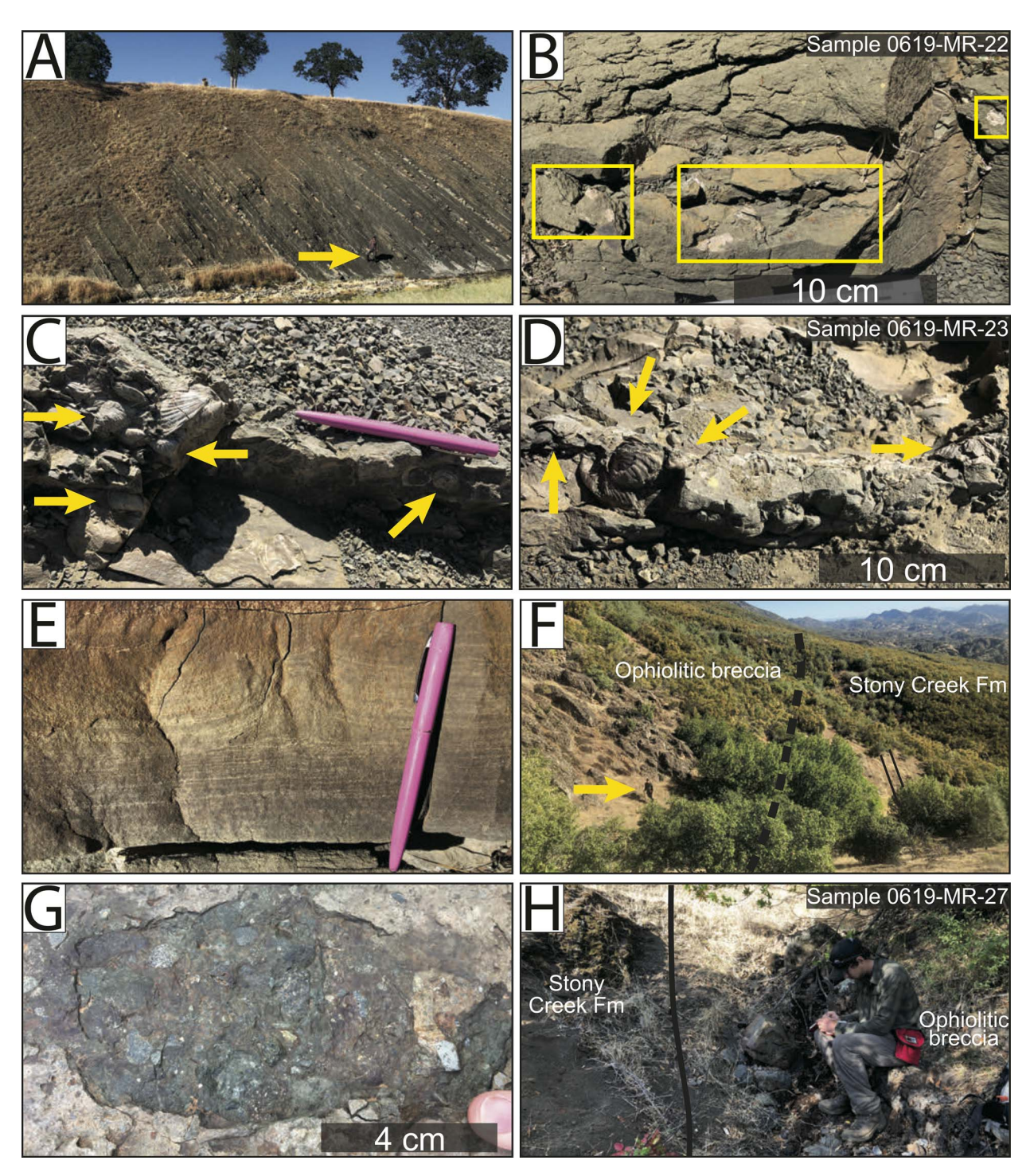


Fig. 7.—Field photos from McCarty Creek (A–E), Crowfoot Point (F–H), Paskenta (I), and Grindstone Creek (J–N) measured sections. A) Outcrop of measured section MC1, within McCarty Creek. View to north; beds dip and young to east. Person for scale (yellow arrow). B) Sandstone bed with bivalves and shell fragments (yellow boxes); sample 0619-MR-22. C) Sandstone bed with Pelecypod Buchia (yellow arrows) and shell fragments. Pink pen is 14 cm long. D) Sandstone bed with Buchia (yellow arrows); sample 0619-MR-23. E) Dewatering structure in sandstone bed. Pink pen for scale. F) Ophiolitic breccia (left) and Stony Creek Formation (right); area of measured section CP1. View to north of beds (solid black lines) of Stony Creek Formation dipping east. Person for scale (yellow arrow). G) Outcrop photo of ophiolitic breccia at sample 06-MR-12 locality highlighting gravel clasts of serpentinite, gabbro, and plagiogranite. H) Contact between ophiolitic breccia (right; sample 0619-MR-27) and Stony Creek Formation (left; sample 0619-MR-28). Person for scale. I) Vertical burrows in sandstone of measured section P01. J) Normally graded sandstone beds and intervening mudstone beds of P01, highlighting sedimentary structures such as plane-parallel lamination overlain by massive sandstone and climbing ripples overlain by plane-parallel lamination. K) Lower measured section GC1, in Grindstone Creek. View to south of beds which dip and young to east. 1.5 m Jacob's staff for scale. L) Top: sandstone with bivalves (black box) in measured section GC1; sample 0619-MR-36. Pink pen is 14 cm long. Bottom: close-up of bivalves. M) Sandstone with bivalve and shell fragments in measured section GC1. Pink pen is 14 cm long. N) Upper part of measured section GC1, in Grindstone Creek. View to north of conglomeratic beds that dip and young to east. Person for scale.

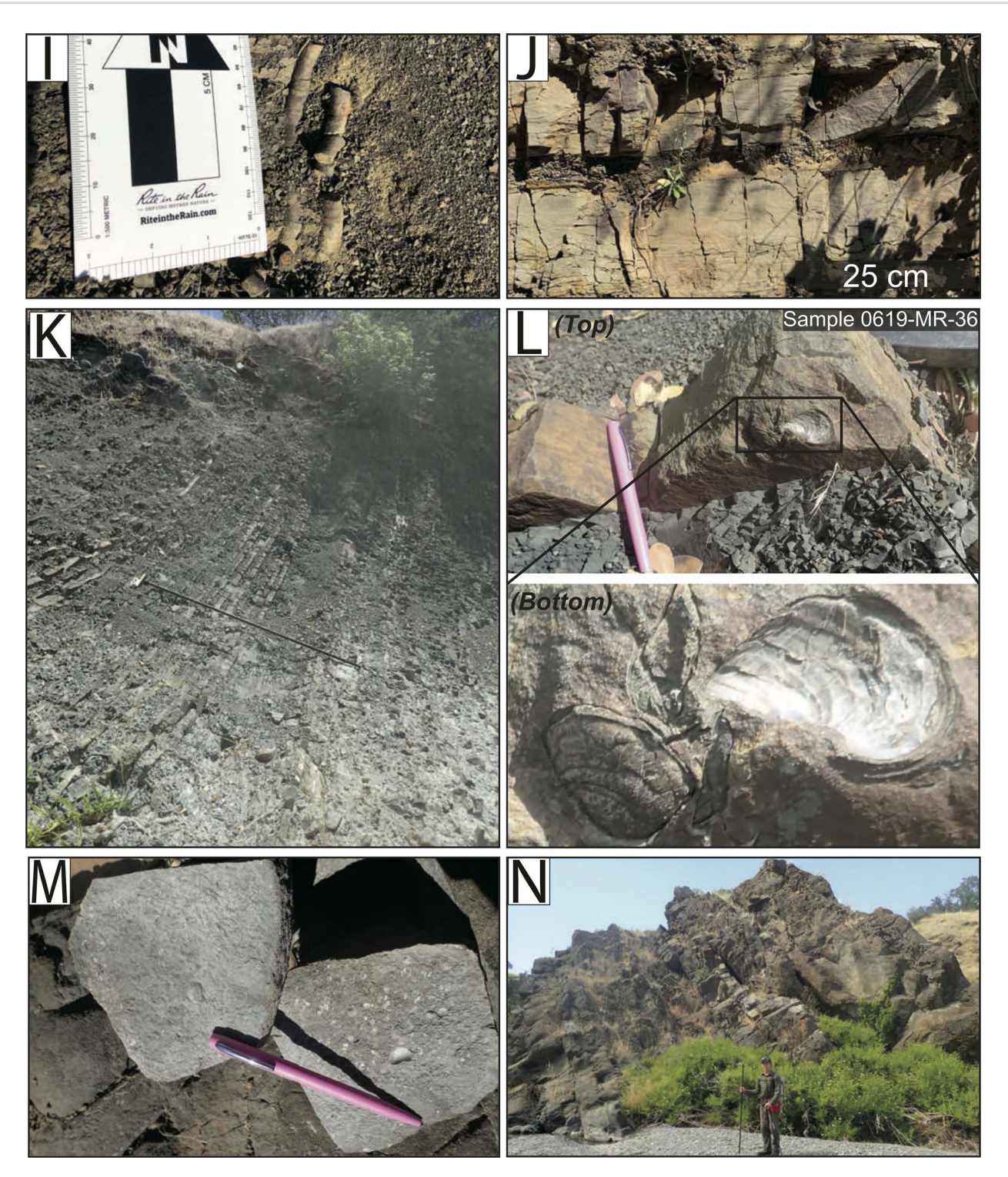


Fig. 7.—Continued.

added in quadrature. Because samples have abundant near-depositional-age grains and therefore MDAs may potentially skew to the young dates on a normal distribution, we interpret the YSP method, which utilizes MSWD values to ensure all grains used in the MDA calculation are part of the same age population (Herriott et al. 2019). In addition, the YSP method is less likely to selectively sample the young tail of a normal distribution than the YGC2 σ (3+) method (Herriott et al. 2019).

RESULTS

Sedimentology and Stratigraphy

We measured five stratigraphic sections along a north–south trend of the northwestern Sacramento basin (Figs. 4, 5). Sections MC1, DC1, CP1, P01, and GC1 range in thicknesses from \sim 15 m to 420 m (Fig. 6). With the exception of Section MC1, stratigraphic sections are limited to the

BLE 1.—Lithofacies a	nd interpretations	Modified after	Ormo et al. (2015)

Lithofacies Code	Description	Interpretation
Gcm	Pebble conglomerate, poorly sorted, clast-supported	Clast-rich or pseudoplastic debris-flow deposits
Gcg	Granule conglomerate, poorly sorted, clast-supported	Clast-rich or pseudoplastic debris-flow deposits
Gmm	Pebble to cobble conglomerate, poorly sorted, matrix-supported	Plastic or cohesive debris-flow deposits (high-strength debris flows)
Gmb	Pebble to cobble breccia, poorly sorted, matrix-supported	Plastic or cohesive debris-flow deposits
Sm	Very fine- to very coarse-grained massive sandstone	Traction carpet during high-density flow. Bouma (1962) Ta; Lowe (1982) S1; Mutti (1992) F8
Sh	Very fine-to very coarse-grained sandstone with plane-parallel lamination	Planar flow bed (upper and lower flow regime); unidirectional flow
Sr	Very fine- to fine-grained sandstone with small ripples	Lower-flow-regime ripples; unidirectional flow
Fsl	Laminated black or gray siltstone	Waning traction sedimentation
Fsm	Massive siltstone	Suspension settling

lowermost strata that are mapped as Jurassic(?) Stony Creek Formation to avoid up-section deformation that might affect our age and provenance determinations for the basal strata. Section MC1 at McCarty Creek characterizes Cretaceous Lodoga Formation (Aptian–Albian) strata structurally above the Paskenta fault zone (Fig. 5A). Section MC1 is included in this study because McCarty Creek is host to one of the most continuously exposed sections in the Paskenta region and allowed us to document up-section changes in provenance.

Facies Descriptions

Measured Section MC1: McCarty Creek.—This 64-m-thick section consists of alternating beds of tan to gray, fine- to medium-grained, moderately sorted sandstone, siltstone, and mudstone (Figs. 6, 7A). Bedforms vary from tabular to lenticular. Lithofacies include massive mudstone (Fsm), laminated siltstone (Fsl), fine- to medium-grained massive sandstone (Sm), and fine- to medium-grained plane-parallellaminated sandstone (Sh). Sandstone and siltstone beds are typically 5–12 cm thick, with a few beds as thick as 40 cm; mudstone intervals are 20-30 cm thick. Fossiliferous sandstone and siltstone beds contain the pelecypod Buchia as well as fragments of unidentified shells commonly in a coquinalike texture (Fig. 7B-D). Fine- to medium-grained massive sandstone beds (Sm) uncommonly have erosional bases. A few sandstone beds contain flame structures and convolute lamination (Fig. 7E). We observed normal grading from medium- to fine-grained sandstone or fine-grained sandstone to siltstone. Toward the top of Section MC1, beds are locally structurally offset at the meter scale.

Measured Section DC1: Digger Creek.—This 43.5-m-thick section primarily comprises gray mudstone beds with relatively few tan to brown, siltstone or fine- to medium-grained, moderately sorted sandstone beds (Fig. 5). Bedforms are mainly tabular and locally lenticular. Lithofacies include massive mudstone (Fsm), laminated siltstone (Fsl), fine- to coarse-grained massive sandstone (Sm), and very fine- to medium-grained plane-parallel-laminated sandstone (Sh). Sandstone and siltstone beds are ~ 10 cm thick. Individual mudstone beds are up to ~ 15 cm thick and commonly amalgamated to form 3–5-m-thick successions of mudstone. A few beds are slightly offset locally in Section DC1. Evidence of soft-sediment deformation is preserved in a siltstone lens near the top of Section DC1.

Measured Section CP1: Crowfoot Point.—Section CP1 records the transition from the ophiolitic breccia to the basal GVG (Figs. 5, 7F–H). This 34-m-thick section consists of a 50-cm-thick matrix-supported pebble–cobble breccia (Gmb) at its base, overlain by alternating beds of tan to brown, very fine- to coarse-grained, poorly sorted sandstone and gray siltstone (Fig. 7F). Clasts in the breccia include basalt, gabbro,

diabase, and chert (Fig. 7G). The Gmb matrix is composed of reddish silty mudstone or sandstone with grains that are angular to subangular. Lithofacies that overlie Gmb include massive mudstone (Fsm), laminated and massive siltstone (grouped as Fsl), very fine- to coarse-grained massive sandstone (Sm), and medium- to coarse-grained plane-parallel-laminated sandstone (Sh). Sandstone and siltstone bed forms are tabular. Sandstone beds are $\sim 5{\text -}10$ cm thick and siltstone beds are up to ~ 15 cm thick

Measured Section P01: Paskenta.—This 14-m-thick section primarily contains alternating beds of buff to brown, very fine- to very coarsegrained, moderately sorted sandstone and siltstone (Fig. 6), with mainly tabular beds. Lithofacies include massive mudstone (Fsm), laminated siltstone (Fsl), very fine- to medium-grained massive sandstone (Sm), very fine- to very coarse-grained plane-parallel-laminated sandstone (Sh), and very fine- to fine-grained sandstone with small ripples (Sr). Sandstone beds are typically 5-10 cm thick, with a few 20-25-cm-thick beds. Near the base of Section P01, sandstone and siltstone beds contain vertical burrows that are ~ 1 cm in diameter (Fig. 7I), along with a mudstone bed that contains brachiopod shell fragments. Evidence for bioturbation is found in a few Sm lithofacies. Tabular sandstone beds commonly fine upward from medium- to fine-grained plane-parallel-laminated sandstone to fine-grained rippled sandstone and massive mudstone (Sh-Sr-Fsm) and from medium- to fine-grained climbing ripples to fine-grained planeparallel-laminated sandstone (Sr-Sh) (Fig. 7J). Flecks of mica and black organic material are observed throughout the section.

Measured Section GC1: Grindstone Creek.—In Grindstone Creek (Fig. 5C), serpentinite mélange is faulted against the Stony Creek Formation and Quaternary alluvium covers the contact between these two units. This 419.1-m-thick composite stratigraphic section was constructed from two measured sections in Grindstone Creek (Fig. 6). The base of Section GC1 is ~ 0.5 km east of the fault contact, at the structurally highest exposure of serpentinite mélange. The lowest 40.5 m of the section consists of alternating beds of tan to gray, fine-grained, moderately sorted sandstone and mudstone (Fig. 7K), with predominantly tabular bed forms. Lithofacies include massive mudstone (Fsm), fine-grained massive sandstone (Sm), fine-grained plane-parallel-laminated sandstone (Sh), and fine-grained sandstone with small ripples (Sr). Sandstone beds are typically 2–5 cm thick, with a rare bed that is ~ 10 cm thick; siltstone intervals range from 5 to 10 cm thick. The pelecypod Buchia is observed in Sr lithofacies that are ~ 10 cm thick, in the lower part of Section GC1 (Fig. 7L). Near the base of the section are a few sandstone and siltstone beds that are locally offset (i.e., < 1.5 meters of broken and discontinuous beds). At 38 m, a 30 cm siltstone with convolute laminations is present

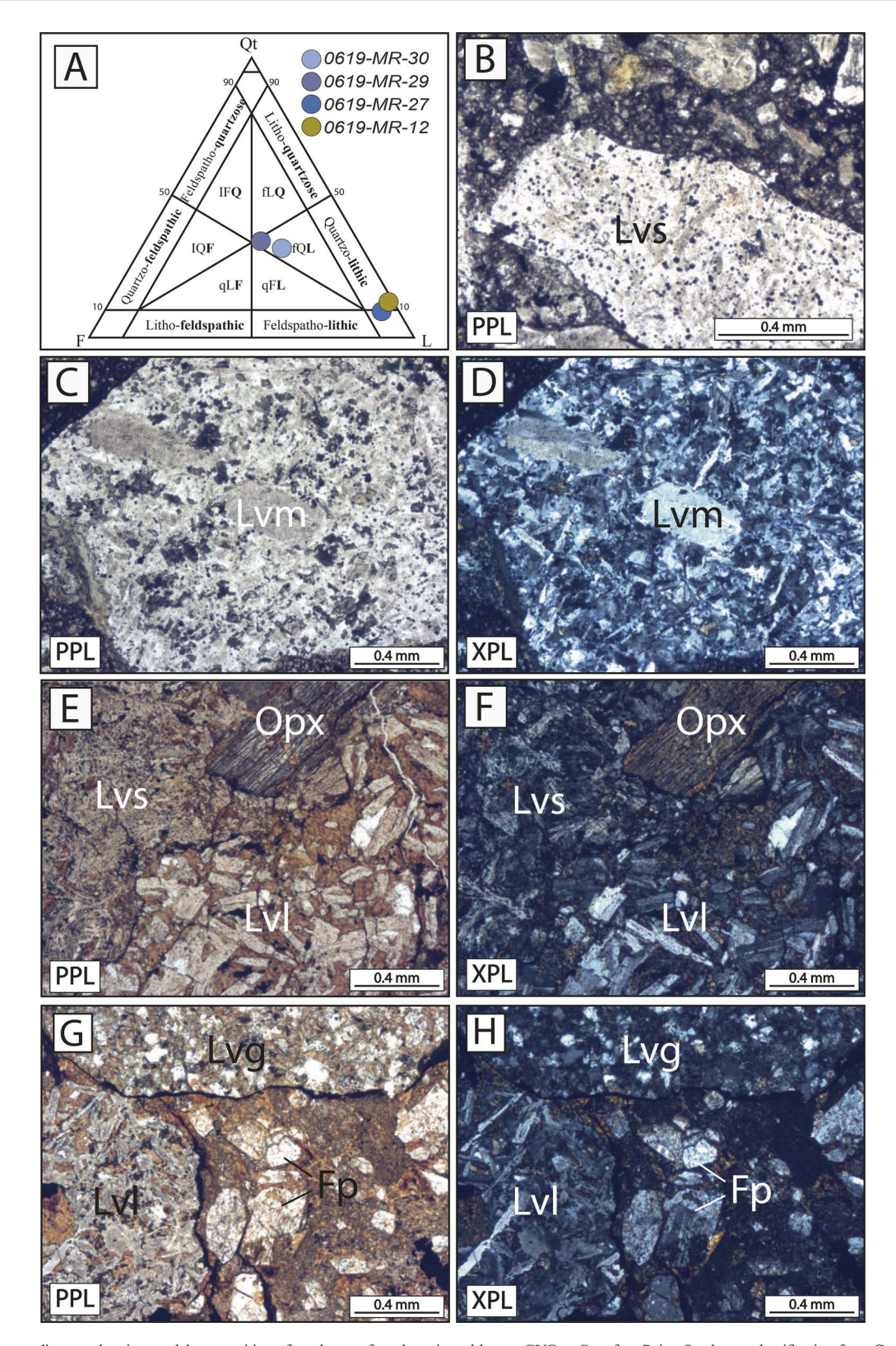


Fig. 8.—A) Ternary diagram showing modal composition of sandstones from breccia and lowest GVG at Crowfoot Point. Sandstone classification from Garzanti (2019). B—H) Photomicrographs of petrofacies from ophiolitic breccia (0619-MR-12, -27) and basal GVG (0619-MR-29, -30), under PPL (Parts B, C, E, G) and XPL (Parts D, F, H). Sample 0619-MR-12 (Parts B, C, D): seriate (Lvs) and microlitic (Lvm) lithic fragments, including plagioclase microlite within pseudomatrix of same material from upper ophiolitic breccia. Sample 0619-MR-27 (Parts E, F): Seriate (Lvs) and lathwork (Lvl) lithic fragments, and orthopyroxene (Opx) from uppermost breccia in contact with GVG in measured section CP1; mechanical compaction evidenced by sutured and concavo-convex grain contacts. Sample 06-10-MR-29 (Parts G, H): granular (Lvg) and lathwork (Lvl) lithic fragments from basal GVG in pseudomatrix; plagioclase (Fp) dissolution and replacement by iron-oxide cements illustrated.

Table 2.—Sample locations in the Sacramento subbasin in northern California.

Sample	Lithology	Unit	Regional Location	Latitude (°N)	Longitude (°W)	Measured Section	U-Pb Analysis	Petrography
0119-MR-01	Sandstone	Stony Creek Formation	Paskenta	39.82008	-122.62507	_	Detrital, n = 305	No
0119-MR-02	Sandstone	Stony Creek Formation	Chrome	39.70809	-122.58168	_	Detrital, $n = 303$	No
P01-3	Sandstone	Stony Creek Formation	Paskenta	39.81484	-122.62901	P01	Detrital, $n = 302$	No
0619-MR-06	Gabbro	Coast Range Ophiolite	Eagle Point	39.92591	-122.64223	_	Igneous, $n = 34$	No
0619-MR-07	Gabbro	Coast Range Ophiolite	Eagle Point	39.9267	-122.64236	_	Igneous, $n = 34$	No
0619-MR-12	Breccia	Ophiolitic breccia	Crowfoot Point	39.88491	-122.62727	_	No Zircon Yield	Yes
0619-MR-14	Sandstone	Stony Creek Formation	Digger Creek	39.89881	-122.62275	DC1	No Zircon Yield	No
0619-MR-15	Sandstone	Stony Creek Formation	Digger Creek	39.89881	-122.62263	DC1	No Zircon Yield	No
0619-MR-16	Sandstone	Stony Creek Formation	Digger Creek	39.89792	-122.61781	_	Detrital, $n = 305$	No
0619-MR-17	Sandstone	Stony Creek Formation	Digger Creek	39.89853	-122.61466	_	Detrital, $n = 309$	No
0619-MR-22	Sandstone	Lodoga Formation	McCarthy Creek	39.91001	-122.56588	MC1	Detrital, $n = 314$	No
0619-MR-23	Sandstone	Lodoga Formation	McCarthy Creek	39.91	-122.56568	MC1	Detrital, $n = 314$	No
0619-MR-24	Sandstone	Lodoga Formation	McCarthy Creek	39.90994	-122.56529	MC1	Detrital, $n = 310$	No
0619-MR-26	Breccia	Ophiolitic breccia	Crowfoot Point	39.89569	-122.62968	_	Detrital, $n = 102$	No
0619-MR-27	Breccia	Ophiolitic breccia	Crowfoot Point	39.88888	-122.62388	CP1	Detrital, $n = 71$	Yes
0619-MR-28	Sandstone	Stony Creek Formation	Crowfoot Point	39.88886	-122.62388	CP1	No Zircon Yield	No
0619-MR-29	Sandstone	Stony Creek Formation	Crowfoot Point	39.88889	-122.6237	CP1	No Zircon Yield	Yes
0619-MR-30	Sandstone	Stony Creek Formation	Crowfoot Point	39.88888	-122.6236	CP1	Detrital, $n = 310$	Yes
0619-MR-35	Sandstone	Stony Creek Formation	Grindstone Creek	39.6769	-122.59036	_	Detrital, $n = 312$	No
0619-MR-36	Sandstone	Stony Creek Formation	Grindstone Creek	39.67575	-122.58553	GC1	Detrital, $n = 305$	No
0619-MR-37	Sandstone	Stony Creek Formation	Grindstone Creek	39.67807	-122.57995	GC1	Detrital, $n = 303$	No

and overlain by 360 m of highly deformed bedding that was measured as cover.

The upper 18.6-m part of Section GC1 consists of beds that are tan to gray, medium- to very coarse, poorly sorted sandstone and siltstone, clastsupported granule conglomerate, clast-supported pebble conglomerate, and matrix-supported pebble-cobble conglomerate (Fig. 6) with mainly tabular bedforms. Lithofacies include massive mudstone (Fsm), laminated siltstone (Fsl), medium- to very coarse-grained massive sandstone (Sm), clast-supported granule conglomerate (Gcg), clast-supported pebble conglomerate (Gcm), and matrix-supported pebble-cobble conglomerate (Gmm). A few beds display Gcg lithofacies that grade normally to Sm lithofacies. Sandstone bed thicknesses are 20-40 cm, with some sandstone beds containing lenses of shale. Siltstone beds are ~ 10 –45 cm thick; some siltstone beds contain sandstone lenses. Shell fragments and the pelecypod Buchia are observed in Sm lithofacies in the upper part of Section GC1 (Fig. 7M). Granule to cobble clasts in the conglomerate beds are primarily red, green, and black chert and sandstone. Conglomerate beds are 70 cm to 3 m thick (Fig. 7N); a few have erosional bases. Tool marks are observed at the bottom of a sandstone bed, near the top part of Section GC1. There are a few channel forms filled with Gmm lithofacies at the top of Section GC1, along with lenses of medium-grained sandstone (Sm) in the Gmm lithofacies.

Depositional Environments

Sections DC1 and CP1, the most basal sections in the northern part of the field area, are dominated by massive mudstone with interbedded siltstone and sandstone. Bedding in DC1 and CP1 is parallel and laterally continuous. We interpret the mudstone to have been deposited by dilute suspensions such as nepheloid flows (e.g., Walker 1965; Lowe 1982). By contrast, siltstone and sandstone beds contain sedimentary structures commonly formed by traction sedimentation (e.g., lithofacies Sh and Sr) and are commonly normally graded. We interpret the siltstone and sandstone facies to have been deposited by distal turbidity flows (e.g., Bouma 1962; Walker 1965; Lowe 1982). Massive to laminated siltstones may reflect suspension sedimentation with near-bed or waning traction effects (e.g., Walker 1965). Based on these facies and outcrop character, we interpret the facies of DC1 and CP1 to have been deposited in a basin-

plain setting. Both sections lack the slumping and contorted beds that would be consistent with deposition on the middle to upper continental slope (e.g., Ingersoll 1978; Suchecki 1984); an exception is the minor convolute bedding at the very top of DC1, which could reflect localized bioturbation or liquefied flow following deposition of the overlying sandstone bed (Lowe 1982).

Sections MC1, P01, and the first 40 m of GC1 are characterized by abundant normally graded sandstones with traction structures and interbedded mudstone and siltstone. Sandstone commonly grades from Sm to Sh-Sr lithofacies and, in two instances, are capped by a heavily burrowed mudstone (P01; Fig. 7I, J). We interpret the sandstone lithofacies as deposited by turbidity flows, with structured sandstone deposited by traction sedimentation and massive or bioturbated mudstone deposited by suspension sedimentation (e.g., Bouma 1962; Walker 1965). We suggest that the 360 m of highly contorted bedding stratigraphically below massive sandstone and clast- and matrix-supported conglomerate beds in GC1 (Fig. 6) was deposited by gravity slumping, such as a masstransport deposit (e.g., Ingersoll 1978, after Walker and Mutti 1973). The conglomerates likely reflect deposition primarily by debris flows, with beds that grade from conglomerate to finer-grained sandstone deposited by turbidity currents (e.g., Middleton and Hampton 1973; Walker 1975; Lowe 1979). Our interpretation is that MC1, P01, and GC1 were deposited along the lower continental slope, consistent with previous interpretations of these strata by Ingersoll (1978) and Suchecki (1984). We favor a lowerslope setting rather than upper slope because gravity slumps commonly accumulate on the lower slope and we did not document any slump scars that would be expected on the upper slope (see models of Ricci-Lucchi 1975).

The stratigraphic position of sections MC1, P01, and the first 40 m of GC1 along strike or just up-section from DC1 and CP1 suggests a close association with basin-plain and lower-slope facies, which were previously documented in Upper Cretaceous GVG strata by Ingersoll (1978, p. 220), who stated "there may have been no clear distinction between lower slope and basin sediments because a uniformly sloping surface may have extended for distances of hundreds of kilometers." Distinguishing these closely related depositional environments in the Upper Jurassic and Lower Cretaceous strata of the GVG is equally difficult, and we collectively

Table 3.—Summary of parameters for modal point counting.

Qt Qm	Total quartzose grains (Qm + Qp) Monocrystalline quartz
Qp	Polycrystalline quartz
F	Total feldspar grains (K + P)
K	Potassium feldspar (microcline, orthoclase, perthite)
P	Plagioclase (Ca and Na varieties)
Fine grain lithic	<u>es</u>
Lm	Total metamorphic lithic grains (Lph + Lsm)
Lph	Phyllite
Lsm	Mica schist
Ls	Total sedimentary lithic grains (C + S + Lc + Lsh)
C	Chert
S	Siltsone
Lc	Carbonate lithic grains
Lsh	Mudstone
Lv	Total volcanic lithic grains (Lvf + Lvl + Lvm + Lvv + Lvx)
Lvf	Felsic volcanic grains (sericite + qtz + feldspar)
Lvl	Lathwork volcanic grains
Lvm	Mafic volcanic grains (epidote $+$ pyx $+$ plag)
Lvv	Vitric volcanic grains
Lvx	Microlitic volcanic grains
Lt	Total lithic grains $(Lm + Ls + Lv + Qp)$
L	Total nonquartzose lithic grains (Lc + Lph + Ls + Lsm + Lv)
Accessory Minerals	amphibole, apatite, biotite, chlorite, epidote, olivine, white mica, zircon

group all stratigraphy studied herein in as basin-plain to lower-slope deposits.

Sandstone Modal Analysis

The average composition (Q₉F₄L₈₇) of sandstone from the matrix of the breccia at Crowfoot Point is dominated by volcanic lithic fragments (Fig. 8A; Table 3), including seriate felsitic (Lvs), microlitic (Lvm), and lathwork (Lvl) grains; microlites in Lvm grains include subhedral to euhedral plagioclase (Fig. 8B-D). We interpret the matrix as pseudomatrix (Dickinson 1970) based on its heterogeneity, poor sorting, and locally fractured volcanic, quartz, and feldspar grains (Fig. 8B). The average composition of two sandstones from the GVG (Q32F28L41) includes more quartz (both monocrystalline and polycrystalline) and feldspar grains than the underlying breccia (See supplemental Material). Lithic grains are felsitic seriate (Lvs) and granular (Lvg) volcanic, lathwork volcanic (Lvl), microlitic volcanic (Lvm), vitric volcanic (Lvv) and one mica schist (Lsm) fragment (Fig. 8E-H). Accessory minerals comprise amphibole, apatite, biotite, chlorite, epidote, olivine, and zircon. Following Garzanti (2016), the matrix of the breccia is quartzo-lithic to lithic sandstone and the GVG sandstone are feldspatho-quartzo-lithic (Fig. 8A). All samples show evidence for mechanical compaction, with sutured, fractured, and concavo-convex grain boundaries. Diagenetic dissolution of plagioclase and replacement by iron-oxide cement is abundant in GVG samples.

Zircon U-Pb Geochronology

Coast Range Ophiolite.—Samples 0619-MR-06 and 0619-MR-07 were collected from outcrops of gabbro near Eagle Peak, west of the Paskenta fault zone (Fig. 5A; Table 2). Zircon U-Pb analysis yields Middle Jurassic weighted mean ages. Sample 0619-MR-06 yields an age of 167.97 ± 1.3 Ma with a

MSWD of 0.63 (n = 28/34). The youngest six grains from Sample 0619-MR-06 are excluded as they form a young tail suggesting that Pb-loss may influence the age; if these ages are included in the calculation the weighted mean has a $p(X^2)$ of 0.003. Sample 0619-MR-07 yields a weighted mean of 165.13 \pm 1.2 Ma with a MSWD of 0.97 (n = 28/34); the five oldest grains form a long tail and were removed from the calculation to yield acceptable MSWD and $p(X^2)$ (see Supplemental Material).

Great Valley Forearc.—Each detrital-zircon sample includes > 300 grains, with the exception of sample 0619-MR-26 (n = 102) and sample 0619-MR-27 (n = 71), which had poor zircon yield (Table 2). All 14 detrital-zircon samples yield U-Pb age spectra containing Precambrian—Mesozoic populations (Fig. 9). Mesozoic age populations consist of age modes at 250–240 Ma, 200–190 Ma, 175–160 Ma, 155–145 Ma, and 140–130 Ma (Fig. 9). Pre-Mesozoic age populations have modes at 2200–2000 Ma, 1900–1600 Ma, 1500–1400 Ma, 1300–950 Ma, 700–550 Ma, and 450–250 Ma (Fig. 9).

Maximum depositional age (MDA) analysis shows good agreement amongst the YGC2 σ (3+), YSP, and MLA methods, with 12 of 14 samples overlapping in age within 2 σ error (Table 4). The YSG commonly does not overlap at 2 σ with other MDA metrics and is not used for interpretation. YSP analyses included between 4 and 111 grains and yielded MSWDs of 0.97–1.03. Two samples, 0619-MR-17 and 06-MR-36, yield MLAs older than the YSP and YGC2 σ (3+), but stratigraphic position indicates that the younger date determined using YSP is more geologically reasonable based on younging up section. Here, we describe the U-Pb age results from all detrital samples by field area, from north to south.

McCarty Creek.—In measured Section MC1, sample 0619-MR-22 is the lowest sample with an MDA of 133.5 \pm 1.5 Ma (Fig. 5A, Table 4). Up-section, samples 0619-MR-23 and 0619-MR-24 yield MDAs of 135.2 \pm 1.4 Ma and 133.2 \pm 1.4 Ma, respectively (Fig. 5A, Table 4). Mesozoic grains comprise 80–96% of the three detrital samples, with age modes at \sim 150 Ma and \sim 135 Ma (Fig. 9).

Digger Creek.—Samples 0619-MR-16 and 0619-MR-17 were collected in Digger Creek, ~ 0.38 km up section of measured Section DC1 and ~ 0.52 km from the contact with the ophiolitic breccia at Crowfoot Point (Fig. 5A). Sample 0619-MR-16 is stratigraphically below sample 0619-MR-17. Samples 0619-MR-16 and 0619-MR-17 yield MDAs of 146.5 \pm 1.7 Ma and 144.4 \pm 2.0 Ma, respectively (Table 4). Mesozoic detrital-zircon grains comprise 53–58% of the two detrital samples, with Mesozoic age modes at \sim 230 Ma, \sim 195 Ma, \sim 165 Ma, and \sim 155 Ma (Fig. 9). Pre-Mesozoic age populations for detrital samples in Digger Creek include \sim 1700–1600 Ma, \sim 1550–1400 Ma, \sim 1300–950 Ma, \sim 420–400 Ma, and \sim 285–265 Ma.

Crowfoot Point.—Sample 0619-MR-26 was collected from sandstone matrix in the lower ophiolitic breccia that overlies the CRO and yields an MDA of 166.1 \pm 1.8 Ma (Fig. 5A, Table 4). Sample 0619-MR-27 was collected from matrix-supported pebble–cobble breccia of the upper ophiolitic breccia and yields an MDA of 150.7 \pm 1.7 Ma (Fig. 5A, Table 4). Mesozoic detrital-zircon ages comprise 92–99% of these two samples, with age modes at \sim 170 Ma, \sim 165 Ma, and \sim 150 Ma (Fig. 9). Sample 0619-MR-30 was collected from the lower strata of the Stony Creek Formation and yields an MDA of 147.1 \pm 1.4 Ma (Fig. 5A, Table 4). This sample contains 98% Mesozoic detrital-zircon ages that form a unimodal age mode at \sim 150 Ma (Fig. 9).

Paskenta.—Sample P01-3 yields an MDA of 148.3 ± 1.5 Ma, and sample 0119-MR-01, collected up-section from P01-3, yields an MDA of 146.8 ± 1.4 Ma (Fig. 5B, Table 4). Mesozoic detrital-zircon grains

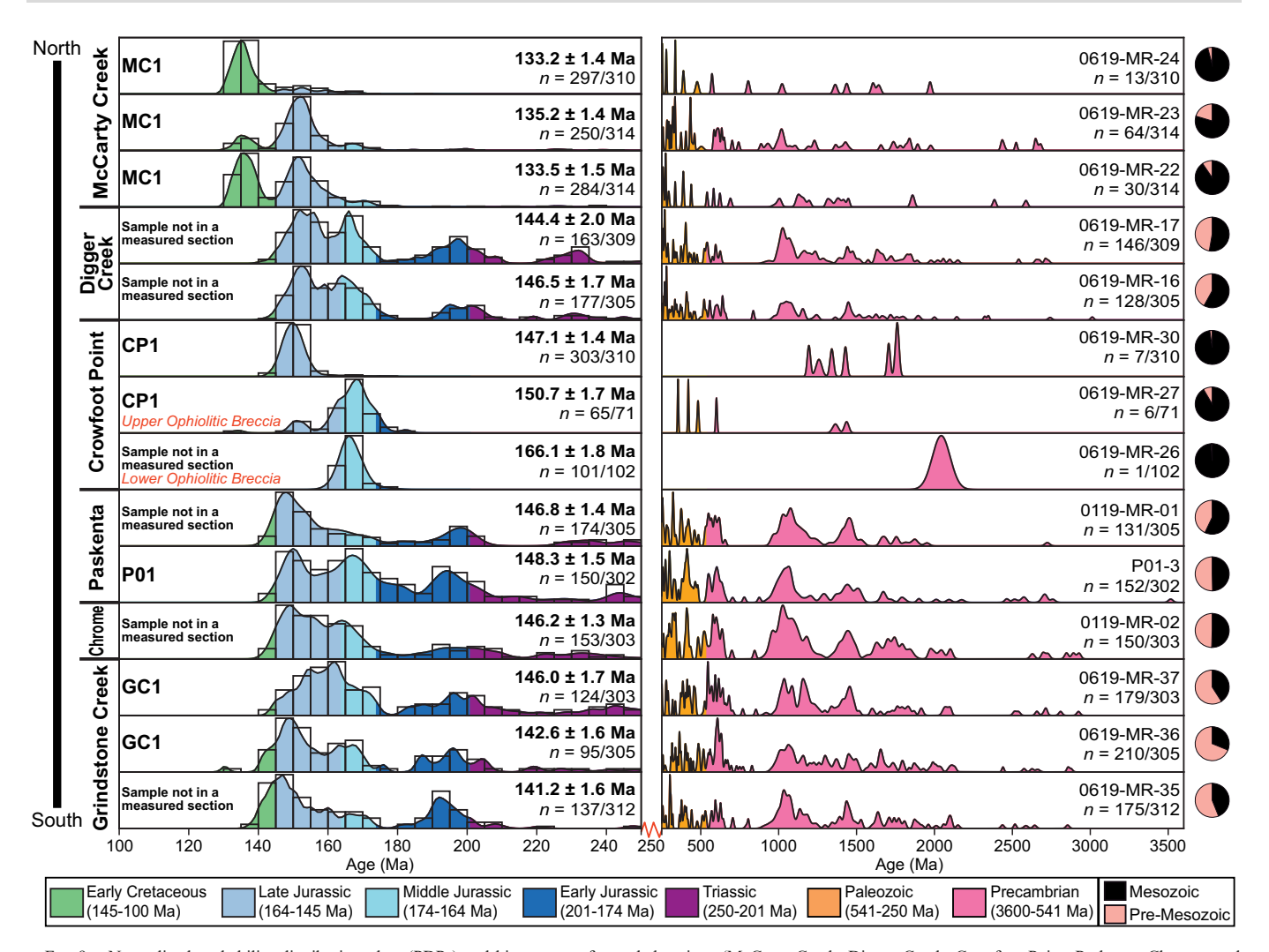


Fig. 9.—Normalized probability distribution plots (PDPs) and histograms of sampled regions (McCarty Creek, Digger Creek, Crowfoot Point, Paskenta, Chrome, and Grindstone Creek) from north to south. Samples are arranged in stratigraphic order in each region, with the oldest sample on bottom. Bolded maximum depositional ages (MDAs) report the youngest statistical age population (YSP). Colors are based on geologic age groupings. Pie diagrams show relative percentages of Mesozoic (black) and pre-Mesozoic (light pink) detrital-zircon ages for each sample. Measured sections: MC1, McCarty Creek; CP1, Crowfoot Point; P01, Paskenta; GC1, Grindstone Creek.

comprise 50–57% of the two detrital samples, with age modes at ~ 245 Ma, ~ 200 Ma, ~ 195 Ma, ~ 167 Ma, and ~ 150 Ma (Fig. 9). Pre-Mesozoic detrital-zircon grains yield age populations of $\sim 1550–1350$ Ma, $\sim 1250–950$ Ma, $\sim 650–500$ Ma, and $\sim 450–300$ Ma.

Chrome.—Sample 0119-MR-02 was collected between measured Section P01 and Section GC1, along Hull Road (i.e., County Road 313, Forest Route 23N05) ~ 4 km southwest of the unincorporated community of Chrome (Fig. 5C), in sandstone ~ 63 m from the uppermost CRO. This sample yields an MDA of 146.2 \pm 1.3 Ma (Table 4) and contains 50% Mesozoic detrital-zircon ages, with age modes at ~ 200 Ma, ~ 165 Ma, and ~ 150 Ma (Fig. 9). The other 50% of detrital-zircon ages are pre-Mesozoic with age populations of $\sim 1850{-}1550$ Ma, $\sim 1500{-}1350$ Ma, $\sim 1250{-}900$ Ma, $\sim 650{-}560$ Ma, $\sim 500{-}400$ Ma, and $\sim 370{-}300$ Ma.

Grindstone Creek.—Sample 0619-MR-35 was collected from an \sim 1-m-thick sandstone bed in Grindstone Creek, \sim 180 m above the contact with the underlying CRO, and yields an MDA of 141.2 \pm 1.6 Ma (Fig. 5C, Table 4). This detrital-zircon sample was obtained down-section of composite measured Section GC1 (Fig. 5C). In the composite measured

Section GC1, sample 0619-MR-36 is the lowest sample with an MDA of 142.6 \pm 1.6 Ma (Fig. 7, Table 4). Sample 0619-MR-37 is located in the upper part of this section and records an MDA of 146.0 \pm 1.7 Ma (Fig. 6, Table 4). Detrital-zircon samples contain 31–44% Mesozoic detrital-zircon ages, with age modes at \sim 242 Ma, \sim 200 Ma, \sim 195 Ma, \sim 187Ma, \sim 170 Ma, \sim 162 Ma, \sim 155 Ma, \sim 150 Ma, and \sim 147 Ma. Pre-Mesozoic detrital-zircon populations include \sim 1800–1600 Ma, \sim 1550–1350 Ma, \sim 1250–950 Ma, \sim 640–550 Ma, and \sim 450–350 Ma (Fig. 9).

DISCUSSION

Sedimentology and Stratigraphy

The lithofacies in stratigraphic sections Digger Creek (DC1), Crowfoot Point (CP1), Paskenta (P01), Grindstone Creek (GC1), and McCarty Creek (MC1) (Fig. 6) are characteristic of deposition by sediment gravity flows (low- and high-density turbidity flows) in basin-plain and lower-continental-slope settings, consistent with previous studies (e.g., Ingersoll 1978, 1982; Suchecki 1984). The Crowfoot Point (CP1) measured stratigraphic section includes the unconformable stratigraphic contact between the upper ophiolitic breccia and the overlying GVG strata (Fig.

TABLE 4.—Calculated maximum depositional age (MDA) using multiple methods for each sample. All errors reported at 2-sigma

		Method 1	Method 2		Method 3		Method 4	
Sample	Assigned Unit	Youngest Single Grain (YSG) (Ma)	Youngest Grain Cluster of 3 or more ages at 2σ , (YGC2 σ 3+) (Ma)	# grains used; MSWD	Youngest Statistical Peak (YSP)	# grains used; MSWD	Maximum Likelihood Age (MLA) (Ma)	Measured Section (Fig. 8)
0119-MR-01	Stony Creek Formation	142.1 ± 3.3	146.0 ± 1.5	n = 37; 0.78	146.8 ± 1.4	n = 54; 1.02	147.7 ± 1.5	
0119-MR-02	Stony Creek Formation	142.8 ± 2.2	146.9 ± 1.2	n = 29; 1.17	146.2 ± 1.3	n = 22; 0.99	147.8 ± 1.3	
P01-3	Stony Creek Formation	143.9 ± 2.0	147.7 ± 1.5	n = 18; 0.91	148.3 ± 1.5	n = 25; 1.00	149.1 ± 1.6	P01-3
0619-MR-16	Stony Creek Formation	142.4 ± 2.2	145.9 ± 1.8	n = 6; 1.03	146.5 ± 1.7	n = 11; 1.03	149.7 ± 1.7	
0619-MR-17	Stony Creek Formation	141.5 ± 2.1	145.4 ± 1.8	n = 7; 1.76	144.4 ± 2.0	n = 4; 1.45	149.4 ± 1.9	1
0619-MR-22	Lodoga Formation	131.0 ± 1.9	133.2 ± 1.5	n = 35; 0.89	133.5 ± 1.5	n = 44; 1.00	134.7 ± 1.5	MC1
0619-MR-23	Lodoga Formation	130.2 ± 1.8	135.2 ± 1.4	n = 26; 1.03	135.2 ± 1.4	n = 26; 1.03	135.3 ± 1.6	MC1
0619-MR-24	Lodoga Formation	130.6 ± 1.9	132.7 ± 1.4	n = 77; 0.78	133.2 ± 1.4	n = 111; 1.00	134.6 ± 1.5	MC1
0619-MR-26	Ophiolitic breccia	160.3 ± 2.5	165.6 ± 1.8	n = 79; 0.72	166.1 ± 1.8	n = 93; 1.01	166.5 ± 1.8	
0619-MR-27	Ophiolitic breccia	134.2 ± 2.1	151.4 ± 1.5	n = 7; 1.4	150.7 ± 1.7	n = 5; 0.97	150.5 ± 3.2	CP1
0619-MR-30	Stony Creek Formation	143.4 ± 1.8	145.9 ± 1.4	n = 42; 0.82	147.1 ± 1.4	n = 105; 1.00	143.4 ± 1.6	CP1
0619-MR-35	Stony Creek Formation	138.1 ± 2.0	141.3 ± 1.6	n = 14; 1.01	141.2 ± 1.6	n = 14; 1.01	143.0 ± 1.7	
0619-MR-36	Stony Creek Formation	130.4 ± 1.8	143.0 ± 1.6	n = 8; 1.34	142.6 ± 1.6	n = 7; 0.91	146.4 ± 1.9	GC1
0619-MR-37	Stony Creek Formation	144.5 ± 2.0	146.7 ± 1.6	n = 8; 1.52	146.0 ± 1.7	n = 6; 1.03	145.8 ± 2.6	GC1

7G, H). Section CP1 also documents an overall up-section shift from deposits of ophiolitic breccia that represent localized cohesive or plastic debris flows (e.g., Lowe 1982; Shultz 1984) to strata of the Stony Creek Formation, which were deposited in deep water by turbidity currents. The matrix-supported pebble–cobble breccia is consistent with the description of the ophiolitic breccia of Lagabrielle et al. (1986) and Robertson (1990), which includes mega-breccia, clast-and matrix-supported conglomerate and breccia, sandstone, and mudstone, and was interpreted to represent ophiolite-derived talus deposited by debris flows.

Pelecypod *Buchia* and shell fragments in turbidite and debris-flow facies occur in the majority of measured stratigraphic sections in strata mapped as Upper Jurassic GVG, leaving open the possibility of downslope transport and contemporaneous reworking of fossils, fragments of fossils, and sediment containing small marine invertebrates. Section MC1, which was measured in strata mapped as the Cretaceous Lodoga Formation, shows a higher abundance of fossiliferous sandstone and siltstone beds that contain the pelecypod *Buchia*, appearing in a coquinalike texture in turbidite facies, not in *in-situ* carbonate seeps as documented by Zakharov and Rogov (2020). These facies in section MC1 document the continuation of clastic deposition primarily by low- and high-density turbidity flows into the Early Cretaceous.

Along Strike Variation in Maximum Depositional Age

In the northernmost part of the study area at Eagle Peak, two samples of gabbro in the upper CRO yield Middle Jurassic zircon U-Pb weighted mean ages of 167.97 \pm 1.3 Ma and 165.13 \pm 1.2 Ma (Fig. 5A, Table 2). South of Eagle Peak, at Crowfoot Point and Digger Creek, samples from the lower and upper ophiolitic breccia that overlies the CRO yield Jurassic MDAs of 166.1 \pm 1.8 Ma (sample 0619-MR-26) and 150.7 \pm 1.7 Ma (sample 0619-MR-27), respectively (Fig. 5A, Table 4). The lower breccia MDA overlaps with the timing of CRO development (173-161 Ma; Mattinson and Hopson 1992; Shervais et al. 2005; Hopson et al. 2008; Orme and Surpless 2019; this study); however, because the lower ophiolitic breccia is primarily locally derived from non-arc sources and reflects the available igneous source material during deposition in the latest Jurassic, it is likely that the TDA of the lower ophiolitic breccia is younger than the mean ages of the CRO. The upper ophiolitic breccia, sampled ~ 520 m up-section, yields an MDA of 150.7 ± 1.7 Ma and a non-unimodal age distribution, consistent with a younger, late Kimmeridgian depositional age for the breccia (timescale of Cohen et al. 2013, updated). Our depositional age result is consistent with the published late Kimmeridgian depositional age for the ophiolitic breccia, which was based on the Buchia rugosa in the Paskenta area (Jones 1975; Pessagno 1977). In this local area at Crowfoot Point (Fig. 5A), a sample from basal GVG, the Stony Creek Formation, unconformably overlies the ophiolitic breccia and yields an MDA of 147.1 ± 1.4 Ma (sample 0619-MR-30), reflecting a maximum duration of ~ 4 Myr for the unconformity (150.7–147.1 Ma), or, incorporating the uncertainties on the MDAs, a range of 0.5 to 6.7 Myr for the duration. We interpret the GVG MDA of \sim 147 as a good approximation for TDA because the next up-section samples yield MDAs of ~ 146 and ~ 144 Ma, younging with stratigraphic position. Generally, the MDAs suggest the duration of the unconformity is slightly less than the > 5 Myr-duration unconformity inferred from other basal GVG locations (Surpless et al. 2006).

Southward, GVG is juxtaposed against serpentinite mélange along a fault contact that potentially omits ophiolitic breccia and basal GVG (Fig. 5B, C). At Paskenta, Chrome, and Grindstone Creek localities, the stratigraphically lowest detrital-zircon samples from strata mapped as Jurassic at each locality yield MDAs of 148.3 ± 1.5 Ma (sample P01-3), 146.2 ± 1.3 Ma (sample 0119-MR-02), and 141.2 ± 1.6 Ma (sample 0619-MR-35), respectively (Figs. 5B, C, 9). Detrital-zircon samples from

northern localities of Chrome, Paskenta, Crowfoot Point, and Digger Creek yield MDAs consistent with deposition during the Jurassic, based on a Jurassic–Cretaceous boundary age of ~ 145.0 Ma (Cohen et al. 2013, updated). In contrast, two of the three samples from Grindstone Creek were deposited during Cretaceous time, including the stratigraphically lowest sample collected adjacent to the serpentinite mélange of the CRO.

Three sandstone samples analyzed for U-Pb geochronology were obtained from Cretaceous strata in the McCarty Creek region located less than 2 km from Jurassic strata to the west (Figs. 4, 5A). The three sandstone samples yield MDAs of ~ 133 Ma and ~ 135 Ma (Fig. 9, Table 4). These Valanginian (or younger) strata up-section from uppermost Jurassic–lowest Cretaceous strata (e.g., Crowfoot Point and Digger Creek localities, MDAs 147–144 Ma) may indicate that motion along the Paskenta fault zone that separates these two sections omitted stratigraphic section.

Provenance Interpretations

Detrital zircon in sedimentary basins may derive from primary sources (first-cycle grains from crystalline and/or igneous sources) and recycled sources (poly-cycle grains from sedimentary sources) (e.g., Schwartz et al. 2019, and references therein). As highlighted by Schwartz et al. (2019), during initiation of the Cordilleran orogen, Paleozoic-lower Mesozoic sedimentary strata covered most North American crustal provinces, suggesting that pre-Sierran-Klamath arc-age grains in the forearc were recycled from sedimentary and crystalline sources that were eroded as the orogen developed. The pre-Mesozoic age spectra of all GVG samples from this study are consistent with recycling from North American sources (Fig. 9), including Laurentian bedrock and North America Cordillera passive-margin strata that collectively comprise detrital-zircon age populations that include 2.85-2.59 Ga, 2.12-2.05 Ga, 1.99-1.74 Ga, 1.85-1.62 Ga, 1.52-1.38 Ga, 1.20-0.97 Ga, 580-490 Ma, and 330-210 Ma (Gehrels and Pecha 2014; Leary et al. 2020, and references therein). Notably, the majority of GVG samples with Late Jurassic and/or earliest Cretaceous MDAs have abundant (often exceeding 50%) pre-Mesozoic grains. By contrast, samples from Lower Cretaceous GVG at McCarty Creek have few pre-Mesozoic-age grains (Fig. 9), consistent with Cretaceous topographic growth of the Sierra Nevada placing the drainage divide within the western terranes of the northern Sierran magmatic arc, as proposed by Ingersoll (1982), Linn et al. (1992), and DeGraaff-Surpless et al. (2002). As the Sierra Nevada arc grew topographically, Early Cretaceous detrital zircon derived from the Sierran magmatic arc dominated the forearc, while the foreland received dominantly recycled Precambrian zircon (e.g., Schwartz et al. 2021).

Proximal to our study region in northern California, the Mesozoic Cordilleran magmatic arc comprises Late Triassic to Late Cretaceous calcalkaline granitoid batholiths and related volcanic rocks of the Sierra Nevada and Klamath mountains (Fig. 10; Bateman and Dodge 1970; Chen and Moore 1982; Bateman 1983; Saleeby and Busby-Spera 1992; Allen and Barnes 2006; Attia et al. 2020, 2021). The Jurassic–Early Cretaceous age populations found in our GVG samples are consistent with first-cycle derivation from these sources (Fig. 10), which is supported by sandstone petrographic results that indicate GVG sandstone are feldspatho-quartzolithic in composition (Fig. 6); the lithic composition is dominated (> 99%) by volcanic grains, including Lvs, Lvg, Lvl, Lvm, and Lvv.

In contrast, the breccia at Crowfoot Point consists of clasts of basalt, gabbro, diabase, and chert in a mudstone to sandstone pseudomatrix that is composed of volcanic lithic grains (e.g., Lvm, Lvl, Lvs; Figs. 6, 7G, 8B–D). Comparison of age distributions from potentially coeval and older igneous sources for the breccia highlight its similarity to the CRO, in contrast to the Sierra Nevada or Klamath Mountains (Fig. 10). In addition to this unimodal peak, sandstone from the breccia also contain six or seven pre-Mesozoic grains, consistent with North American affinity. The GVG sandstone immediately overlying the breccia also has a unimodal

age peak and few (n = 7) pre-Mesozoic grains. Integrated with the composition of clasts and framework grains from the matrix, we interpret the breccia to be derived from erosion of the ophiolite, proximal to North America and in a spatially limited drainage catchment that contained latest Jurassic plutons of the Sierra Nevada–Klamath magmatic arcs. Unimodal age peaks in GVG strata are also found in Upper Cretaceous strata (e.g., Venado Formation) and interpreted as point-source derived (DeGraaff-Surpless et al. 2002).

Tectonic Implications

We propose a tectonic model for early development of the northwestern Sacramento basin during Late Jurassic-earliest Cretaceous time (Fig. 11). Ophiolitic breccia and basal strata of the Stony Creek Formation contain pre-Mesozoic and Mesozoic detrital zircon of North American affinity, supporting the interpretation that they were deposited proximal to the Sierra Nevada-Klamath magmatic arcs. The composition of clasts and framework grains of the breccia, and its igneous U-Pb dates, support derivation from the CRO. We interpret the ophiolitic breccia to have been deposited by \sim 151 Ma (Fig. 11A), during faulting resulting from localized dismemberment and uplift of the middle Jurassic CRO (Hopson et al. 1981; Robertson 1990). This interpretation is consistent with Hopson et al. (2008), who first proposed that dismembered oceanic crust developed large structural relief via faulting that occurred before, during, and after breccia deposition. However, our model differs from Hopson et al. (2008), as we interpret the dismemberment to be in a forearc position, not an open ocean. The interpretation that the upper ophiolitic breccia formed in a forearc position immediately before, prior to GVG deposition, is consistent with models that invoke the beginning of GVG deposition in a forearc-basin setting, following arc-arc collision (i.e., Nevadan orogeny) (e.g., Schweickert and Cowan 1975; Ingersoll 1982).

We further suggest that deformation of the CRO and initial sedimentation of the GVG occurred during two phases of forearc extension proximal to North America, based on several lines of evidence. First, there is significant attenuation of the CRO at the latitude of our study area (Fig. 4) and westward thickening and onlap of the Stony Creek Formation onto the CRO (Fig. 11A). Subsurface seismic imaging at the latitude of Paskenta shows ~ 6 km of structural relief of the CRO (Constenius et al. 2000, their Fig. 8C). Integrating these observations with our age and provenance data, we suggest that normal faulting during the earliest stages of forearc deposition (~ 151-140 Ma) generated steep bathymetric relief of the CRO surface and produced the accommodation space for the ophiolitic breccia and forearc-basin sediments (Fig. 11A). An extensional mechanism to explain thinning of the CRO is also supported by the lack of folding, contractional faulting of the CRO, or thrust duplication of the CRO before deposition of ophiolitic breccia (e.g., Robertson et al. 1990), and serpentinite diapirism during the earliest Cretaceous (Wakabayashi 2019). Our inference that structural relief of the CRO resulted from extension is consistent with the interpreted localized provenance for the lower breccia with limited North American crustal input, versus a wider catchment geometry for the upper breccia and basal GVG that would incorporate more detritus from the Sierra Nevada-Klamath magmatic arcs and pre-batholith framework (e.g., Orme and Surpless 2019).

As extension progressed, the structural level of normal faulting stepped up to the top of the Stony Creek Formation and the faults in the Paskenta, Cold Fork, and Elder Creek fault zone began (Fig. 11B). These fault systems governed the development of a syndepositional half-graben system in the forearc basin, as indicated by stratal thickening and Valanginian—Turonian GVG strata in the hanging wall of the Paskenta fault zone, as well as the Elder Creek and Cold Fork fault zones to the north (Fig. 4; Constenius et al. 2000). Onlap of the Lower Cretaceous Lodoga Formation onto the CRO highlights the syndepositional motion

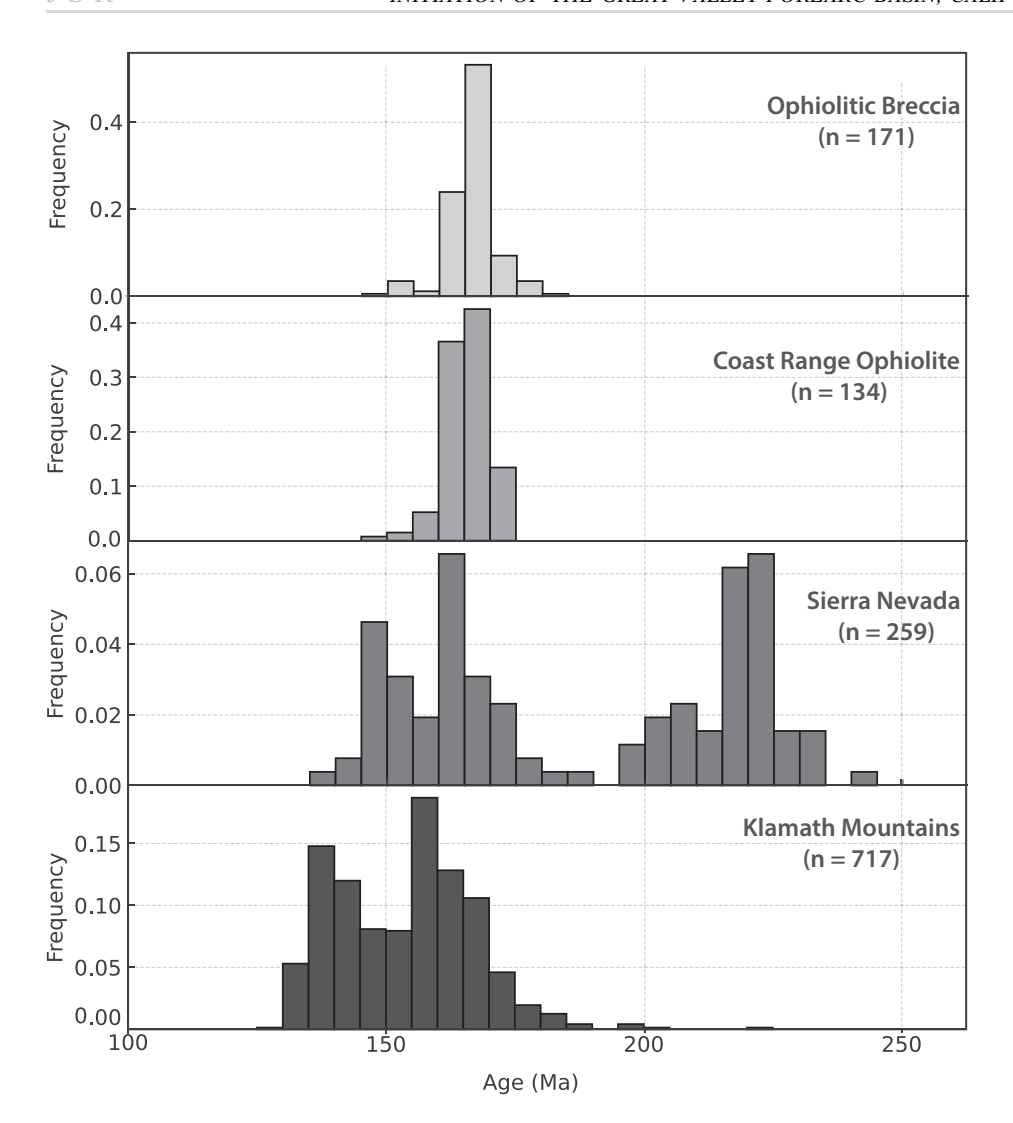


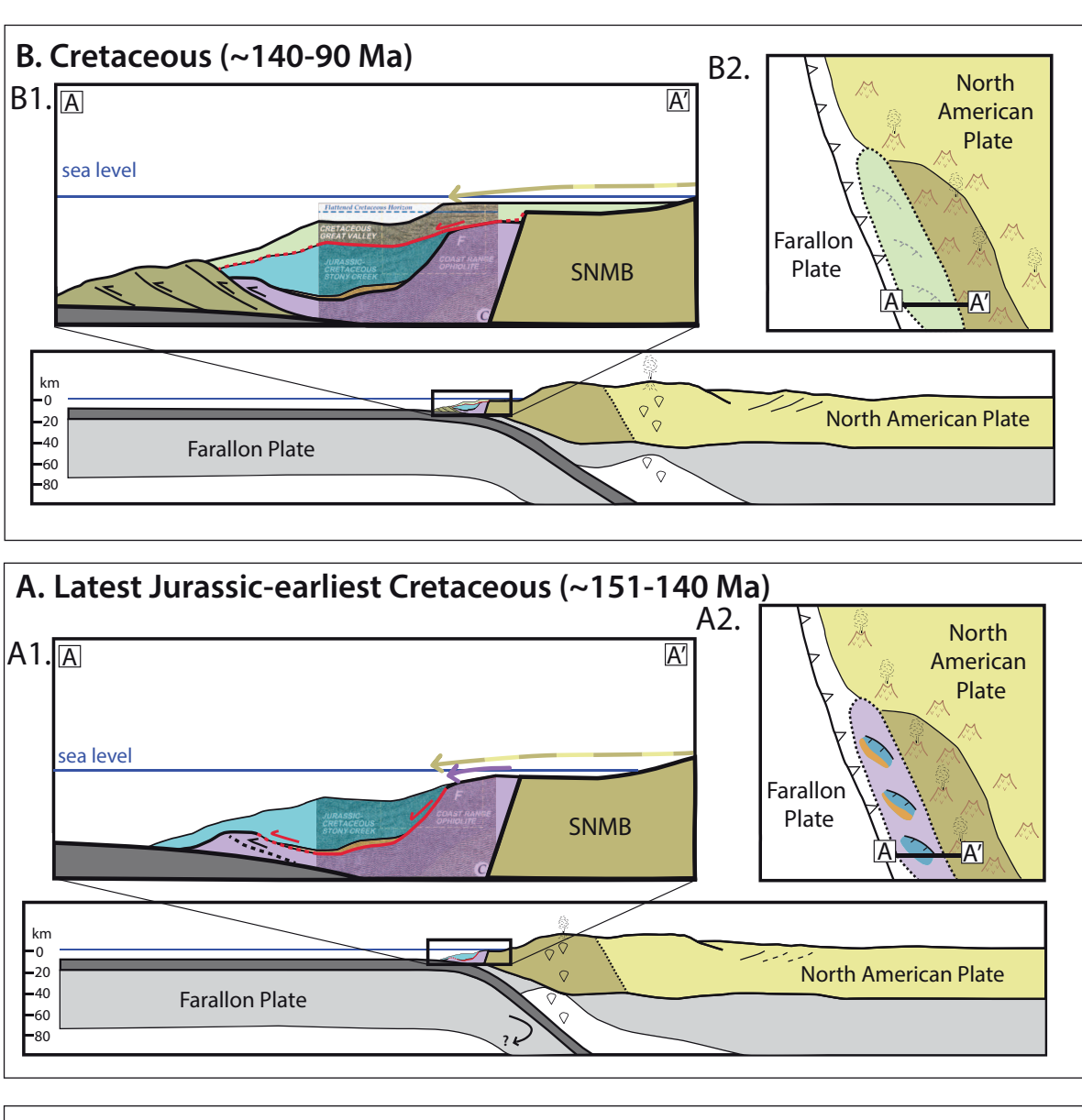
Fig. 10.—Histograms of igneous U-Pb dates compiled from the Klamath Mountains, Sierra Nevada Mountains, Coast Range Ophiolite, and ophiolitic breccia (this study), restricted to dates between 250–125 Ma, as younger GVG strata are not part of this study. References for Coast Range Ophiolite near Paskenta: Saleeby et al. 1989; Shervais et al. 2005; Orme and Surpless 2019; this study. References for Sierra Nevada: Stern et al. 1981; Saleeby et al. 1989; Tobisch et al. 2000; Barth et al. 2011; Cao et al. 2015, 2016; Ardill et al. 2018; Barth et al. 2018; Ratschbacher et al. 2018; Attia et al. 2020, and references therein. References for Klamath Mountains: Allen and Barnes 2006; Surpless et al. 2023, and references therein.

along the Paskenta fault system (Fig. 11B). We interpret the latest Jurassic–earliest Cretaceous segmented depocenters to have filled during Early Cretaceous time, forming an integrated forearc basin (Fig. 11B) (DeGraaff-Surpless et al. 2002; Orme and Surpless 2019). As the basin widened during the earliest Late Cretaceous (e.g., Ingersoll 1982), sediments of the GVG onlapped eastward onto the Sierra Nevada metamorphic belt (Fig. 11B; Orme and Graham 2018) and motion along the normal fault systems ceased during Turonian time (~ 90 Ma) (Constenius et al., 2000).

The timing of the initial phase of extension proposed by this study (~ 151 –140 Ma) and by Constenius et al. (2000) overlaps with the timing of latest Jurassic contractional deformation that is documented in the western Sierran foothills and Klamath Mountains, termed the Nevadan orogeny (e.g., Schweickert 2015). Deformation and metamorphism of the Upper Jurassic Galice Formation in the Klamath Mountains ~ 155 –150 Ma (Harper et al. 1994; Hacker et al. 1995; MacDonald et al. 2006) and the Upper Jurassic Mariposa Formation in the western foothills of the Sierra Nevada ~ 152 Ma (Bogen 1984; Snow and Ernst 2008), and intrusion of the ~ 151 –149 Ma Guadalupe Igneous Complex (Saleeby et al. 1989; Ernst et al. 2009; Ratschbacher et al. 2018) support regional contraction in the latest Jurassic (155–145 Ma) (Paterson et al. 1991; Haeussler and Paterson 1993; Paterson and Miller 1998).

This latest Jurassic contraction in the Sierra Nevada foothills during the Nevadan orogen was followed by a westward shift in magmatism as Franciscan subduction was established along the western margin of newly accreted arc terranes (Schweickert 2015; Ingersoll 2019, and references therein). In this model, extension in the newly formed GVf basin may have been related to establishment of Franciscan subduction in latest Jurassic time, following arc–arc collision. We note that the Franciscan accretionary prism is interpreted to have been non-accretionary until $\sim 20{\text -}25$ Myr after GVG deposition began (Dumitru et al. 2010; DeCelles and Graham 2015), implying the existence of a non-contractional mechanism to capture sediment from the eroding North American margin in a forearc basin during the latest Jurassic onset of basin development.

Coeval extension and contraction are common along modern forearc regions experiencing oblique subduction, such as the Sumatra–Java and Mariana forearc systems (e.g., Schlüter et al. 2002; Heeszel et al. 2008). The Jurassic magmatic arc of the western U.S. Cordillera was broadly characterized by extension before latest Jurassic—earliest Cretaceous intraarc shortening (e.g., Saleeby and Busby-Spera 1992; Busby 2012; Seton et al. 2012; Saleeby and Dunne 2015), overlapping with the timing of proposed extension and deposition of the breccia in northern California. Proposed synchronous forearc extension and magmatic arc contraction during the Late Jurassic—Early Cretaceous may be analogous to the modern outer forearc of the northern Chilean margin, which is experiencing extension synchronous with compression in the western margin of the active magmatic arc (Reuther and Adam 1996; Adam and Reuther 2000).



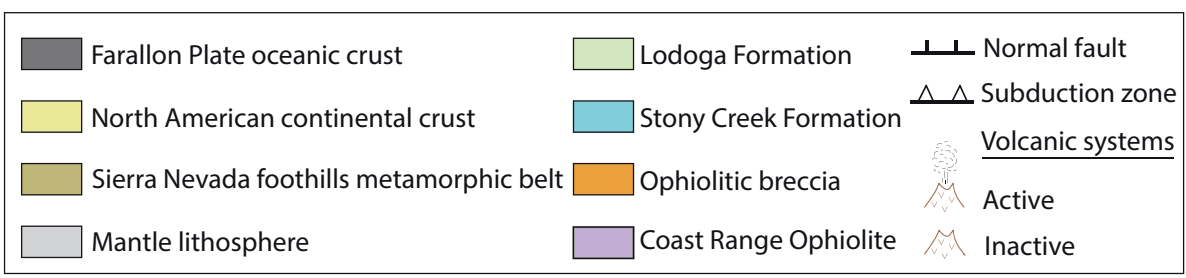


Fig. 11.—Schematic tectonic model for deposition of ophiolitic breccia, latest Jurassic–earliest Cretaceous Stony Creek Formation, and Early to earliest Late Cretaceous GVG sediments during initial stages of development of Great Valley forearc basin. A) Cross section (A1) and map view (A2) at ~ 151 –140 Ma: deposition of ophiolitic breccia (orange) and oldest GVG, the Stony Creek Formation (blue) in isolated fault-controlled depocenters of the forearc region. Seismic line TX-3 from Constenius et al. 2000, their Figure 8C (indicated by darker shading) is included as a guide for preserved architecture. Geometry toward the trench is inferred to explain trapping of sediment and informed by modern forearc systems that show normal and reverse faulting in forearc basin and subduction interface, respectively (e.g., Noda and Miyakawa 2016). B) Cross section (B1) and map view (B2) at ~ 144 –133 Ma: segmented depocenters are overfilled with continued GVG deposition (light green) and form a cohesive forearc basin. Note that GVG deposition atop the Sierran Foothills does not occur until ~ 100 –90 Ma, consistent with subsurface studies (e.g., Moxon 1988; Orme and Graham 2018). The blue line indicates sea level, following Williams (1997). Tectonic models are to scale, modified after Ingersoll (2019) and Orme and Surpless (2019). SNMB, Sierra Nevada Metamorphic belt.

CONCLUSIONS

The upper ophiolitic breccia in northern California was deposited between ~ 151 and ~ 147 Ma, atop the Middle Jurassic CRO (~ 164 Ma), < 4 Myr before the onset of GVG sedimentation; the lower ophiolitic breccia may have been deposited as early as ~ 166 Ma. Jurassic MDAs along with the presence of pre-Mesozoic and Mesozoic detritalzircon ages in the ophiolitic breccia suggest deposition in a forearc position proximal to the Sierra Nevada-Klamath magmatic arc of North America. We propose a model whereby extensional dismemberment of the CRO may have generated high bathymetric relief and isolated faultbounded depocenters that trapped sediment during early development of the GVf (Fig. 11A). We suggest that variation in maximum depositional ages from basal strata (Stony Creek Formation) of the GVf at Digger Creek, Crowfoot Point, Paskenta, Chrome, and Grindstone Creek reflect diachronous deposition in these segmented depocenters during early development of the Sacramento basin between 151 and 140 Ma. Subsequently, during the middle Early Cretaceous, the structural level of normal faulting stepped up to atop the Stony Creek Formation, and a new system of syndepositional normal faults governed the focus of deposition (Fig. 11B). These latest Jurassic-earliest Cretaceous isolated depocenters were filled by the end of the Early Cretaceous, forming a coherent forearc basin that collected detritus from sources in the Klamath-Sierra Nevada magmatic arc as the forearc-arc system matured.

SUPPLEMENTAL MATERIAL

A supplemental file is available from the SEPM Data Archive: https://www.sepm.org/supplemental-materials.

ACKNOWLEDGMENTS

Funding was provided by the National Science Foundation (NSF) grant EAR-1942460 to D.A. Orme and the NSF Graduate Research Fellowship Program (GRFP) under grant 419-2034 to M.C. Romero. This research was also supported by a Geological Society of America Graduate Student Research Grant, Northern California Geological Society Richard Chambers Memorial Scholarship, and a Montana State University Marathon Oil Scholarship to M.C. Romero. We thank the University of Arizona LaserChron Center staff for analytical support (NSF grant EAR-1649254), GeoSep Services (GSS) and ZirChron for mineral separation. We thank Snir Attia and Kurt Sundell for generously sharing a compilation of U-Pb ages from the central Sierra Nevada and the DZmda code before publication, respectively. We thank James Gleason and Jessica Zehner for general feedback on Figure 11. We especially thank the ranchers and landowners of the Paskenta and Grindstone Creek areas for facilitating field work. We are grateful to Associate Editor Raymond Ingersoll, and reviewers Theresa Schwartz, Scott Johnston, Kurt Constenius, and Jeffrey Trop for feedback on the manuscript.

REFERENCES

- ADAM, J., AND REUTHER, C. D., 2000, Crustal dynamics and active fault mechanics during subduction erosion: application of frictional wedge analysis on to the North Chilean Forearc: Tectonophysics, v. 321, p. 297–325, doi:10.10116/S0040-1951(00)00074-3.
- ALLEN, C.M., AND BARNES, C.G., 2006, Ages and some cryptic sources of Mesozoic plutonic rocks in the Klamath Mountains, California and Oregon, *in* Snoke, A.W., and Barnes, C.G., eds., Geological Studies in the Klamath Mountains Province, California and Oregon: A Volume in Honor of William P. Irwin: Geological Society of America, Special Paper 410, p. 223–245, doi:10.1130/2006.2410(11).
- ALMGREN, A.A., AND HACKER, P.D., eds., 1984, Paleogene Submarine Canyons of the Sacramento Valley, California: Bakersfield, California: American Association of Petroleum Geologists, Pacific Section, Symposium Volume 1, 187 p.
- Ardill, K.A., Paterson, S.R., and Memeti, V., 2018, Spatiotemporal magmatic focusing in upper-mid crustal plutons of the Sierra Nevada arc: Earth and Planetary Science Letters, v. 498, p. 88–100, doi:10./1016/j.epsl.2018.06.023.
- ATTIA, S., COTTLE, J.M., AND PATERSON, S.R., 2020, The erupted zircon record of continental crust formation during mantle driven arc flare-ups: Geology, v. 48, p. 446–451, doi:10.1130/G46991.1.

- ATTIA, S., PATERSON, S.R., SALEEBY, J., AND CAO, W., 2021, Detrital zircon provenance and depositional links of Mesozoic Sierra Nevada intra-arc strata: Geosphere, v. 17, p. 1422– 1453, doi:10.1130/GES02296.1.
- Balley, E.H., AND Blake, M.C., Jr., 1974, Major chemical characteristics of Mesozoic Coast Range ophiolite in California: U.S. Geological Survey, Journal of Research, v. 2, no. 6, p. 637–656.
- BAILEY, E.H., BLAKE, M.C., JR., AND JONES, D.L., 1970, On-land Mesozoic oceanic crust in California Coast Ranges, in Geological Survey Research 1970, Chapter C: U.S. Geological Survey, Professional Paper 700-C, p. 70–81.
- Barth, A.P., Walker, J.D., Wooden, J.L., Riggs, N.R., and Schweickert, R.A., 2011, Birth of the Sierra Nevada magmatic arc: early Mesozoic plutonism and volcanism in the east-central Sierra Nevada of California: Geosphere, v. 7, p. 877–897, doi:10.1130/GES00661.1.
- BARTH, A.P., WOODEN, J.L., RIGGS, N.R., WALKER, J.D., TANI, K., PENNISTON-DORLAND, S.C., JACOBSON, C.E., LAUGHLIN, J.A., AND HIRAMATSU, R., 2018, Marine volcaniclastic record of early are evolution in the Eastern Ritter Range pendant, Central Sierra Nevada, California: Geochemistry, Geophysics, Geosystems, v. 19, p. 2543–2559, doi:10.1029/2018GC007456.
- BATEMAN, P.C., 1983, A summary of critical relations in the central part of the Sierra Nevada batholith, California, U.S.A., *in* Roddick, J.A., ed., Circum-Pacific Plutonic Terranes: Geological Society of America, Memoir 159, p. 241–254, doi:10.1130/MEM159-p241.
- BATEMAN, P.C., AND DODGE, F.C.W., 1970, Variations of major chemical constituents across the central Sierra Nevada batholith: Geological Society of America, Bulletin, v. 81, p. 409–420, doi:10.1130/0016-7606(1970)81[409:VOMCCA]2.0.CO;2.
- Bertucci, P.F., 1983, Petrology and provenance of the Stony Creek Formation, northwestern Sacramento Valley, California, *in* Bertucci, P.F., and Ingersoll, R.V., eds., Guidebook to the Stony Creek Formation, Great Valley Group, Sacramento Valley, California: SEPM, Pacific Section, p. 1–16.
- Bezore, S.P., 1969, The Mount St. Helens ultramafic-mafic complex of the northern Coast Ranges [Abstract]: Geological Society of America, Abstracts with Programs, v. 1, p. 5.
- BLAKE, M.C., JR., JAYKO, A.S., JONES, D.L., AND ROGERS, B.W., 1987, Unconformity between Coast Range Ophiolite and part of the lower Great Valley Sequence, South Fork of Elder Creek, Tehama County, California, *in* Hill, M.L., ed., Centennial Field Guide: Geological Society of America, Cordilleran Section, v. 1, p. 279–282.
- BLAKE, M.C., JR., HELLEY, E.J., JAYKO, A.S., JONES, D.L., AND OHLIN, H.N., 1992, Geologic map of the Willows 1:100,000 quadrangle, California: U.S. Geological Survey, Open-File Report, no. 92–271, doi:10.3133/off92271.
- BOGEN, N.K., 1984, Stratigraphy and sedimentary petrology of the Upper Jurassic Mariposa Formation, western Sierra Nevada, California, in Crouch, J.K., and Bachman, S.B., eds., Tectonics and Sedimentation along the California Margin: SEPM, Pacific Section, Book 38, p. 119–134.
- BOUMA, A.H., 1962, Sedimentology of Some Flysch Deposits: A Graphic Approach to Facies Interpretations: Amsterdam, Elsevier, 168 p.
- BUSBY, C.J., 2012, Extensional and transtensional continental arc basins: case studies from the southwestern United States, in Busby, C., and Azor, A., eds., Tectonics of Sedimentary Basins: Recent Advances: Oxford, Blackwell Publishing, p. 382–404, doi:10.1002/9781444347166.ch19.
- CADY, J.W., 1975, Magnetic and Gravity Anomalies in the Great Valley and Western Sierra Nevada Metamorphic Belt, California: Geological Society of America, Special Paper 168, 56 p., doi:10.1130/SPE168-p1.
- CAO, W., AND PATERSON, S.R., 2016, A mass balance and isostasy model: exploring the interplay between magmatism, deformation and surface erosion in continental arcs using central Sierra Nevada as a case study: Geochemistry, Geophysics, Geosystems, v. 17, p. 2194–2212, doi:10.1002/2015GC006229.
- CAO, W., PATERSON, S.R., MEMETI, V., MUNDIL, R., ANDERSON, L., AND SCHMIDT, K., 2015, Tracking paleodeformation fields in the Mesozoic central Sierra Nevada arc: implications for intra-arc cyclic deformation and arc tempos: Lithosphere, v. 7, p. 296–320, doi:10. 1130/L389.1.
- CHEN, J.H., AND MOORE, J.G., 1982, Uranium-lead isotopic ages from the Sierra Nevada batholith, California: Journal of Geophysical Research, v. 87, p. 4761–4784, doi:10. 1029/JB087iB06p04761.
- CLIFT, P.D., AND VANNUCCHI, P., 2004, Controls on tectonic accretion versus erosion in subduction zones: implications for the origin and recycling of the continental crust: Reviews of Geophysics, v. 42, p. 1–31, doi:10.1029/2003RG000127.
- COHEN, K.M, FINNEY, S.C., GIBBARD, P.L., AND FAN, J.-X., 2013 (updated), The ICS International Chronostratigraphic Chart: Episodes, v. 36, p. 199–204.
- Constenius, K.N., Johnson, R.A., Dickinson, W.R., and Williams, T.A., 2000, Tectonic evolution of the Jurassic–Cretaceous Great Valley forearc, California: implications for the Franciscan thrust-wedge hypothesis: Geological Society of America, Bulletin, v. 112, p. 1703–1723, doi:10.1130/0016-7606(2000)112<1703:TEOTJC>2.0.CO;2.
- COUTTS, D.S., MATTHEWS, W.A., AND HUBBARD, S.M., 2019, Assessment of widely used methods to derive depositional ages from detrital zircon populations: Geoscience Frontiers, v. 10, p. 1421–1435, doi:10.1016/j.gsf.2018.11.002.
- DeCelles, P.G., and Graham, S.A., 2015, Cyclical processes in the North American Cordilleran orogenic system: Geology, v. 43, p. 499–502, doi:10.1130/G36482.1.
- DeGraaff-Surpless, K., Graham, S.A., Wooden, J.L., and McWilliams, M.O., 2002, Detrital zircon provenance analysis of the Great Valley Group, California: evolution of

- an arc-forearc system: Geological Society of America, Bulletin, v. 114, p. 1564–1580, doi:10.1130/0016-7606(2002)114<1564:DZPAOT>2.0.CO;2.
- DEPAOLO, D.J., 1981, A neodymium and strontium isotopic study of the Mesozoic calcalkaline granitic batholiths of the Sierra Nevada and Peninsular Ranges, California: Journal of Geophysical Research, v. 86, p. 10,470–10,488. doi:10.1029/JB086iB11p10470
- DICKINSON, W.R., 1970, Interpreting detrital modes of graywacke and arkose: Journal of Sedimentary Petrology, v. 40, p. 695–707, doi:10.1306/74D72018-2B21-11D7-8648000102C1865D.
- DICKINSON, W.R., 1985, Interpreting provenance relations from detrital modes of sandstones. in Zuffa. G.G., ed., Provenance of Arenites: Dordrecht, Reidel, p. 333–361.
- DICKINSON, W.R., 1995, Forearc basins, in Busby, C.J., and Ingersoll, R.V., eds., Tectonics of Sedimentary Basins: Cambridge, Blackwell, p. 221–261.
- DICKINSON, W.R., AND GEHRELS, G.E., 2009, Use of U-Pb ages of detrital zircons to infer maximum depositional ages of strata: a test against a Colorado Plateau Mesozoic database: Earth and Planetary Science Letters, v. 288, p. 115-125.
- DICKINSON, W.R., AND RICH, E.I., 1972, Petrologic intervals and petrofacies in the Great Valley sequence, Sacramento Valley, California: Geological Society of America, Bulletin, v. 83, p. 3007–3024, doi:10.1130/0016-7606(1972)83[3007:PIAPIT]2.0.CO;2.
- Dickinson, W.R., And Seely, D.R., 1979, Structure and stratigraphy of forearc regions: American Association of Petroleum Geologists, Bulletin, v. 63, p. 2–31.
- DICKINSON, W.R., HOPSON, C.A., AND SALEEBY, J.B., 1996, Alternate origins of the Coast Range Ophiolite (California): introduction and implications: Geological Society of America, Geology Today, v. 6, p. 2–10.
- DUMITRU, T.A., WAKABAYASHI, J., WRIGHT, J.E., AND WOODEN, J.L., 2010, Early Cretaceous transition from nonaccretionary behavior to strongly accretionary behavior within the Franciscan subduction complex: Tectonics, v. 29, no. TC5001, doi:10.1029/2009TC002542
- ENGEBRETSON, D.C., COX, A., AND GORDON, R.G., 1985, Relative motions between oceanic and continental plates in the Pacific Basin: Geological Society of America, Special Paper 206, 59 p.
- ERNST, W.G., 1970, Tectonic contact between the Franciscan mélange and the Great Valley sequence: crustal expression of a late Mesozoic Benioff zone: Journal of Geophysical Research, v. 75, p. 886–901, doi:10.1029/JB075i005p00886.
- ERNST, W.G., SALEEBY, J.B., AND SNOW, C.A., 2009, Guadalupe pluton: Mariposa Formation age relationships in the southern Sierra Foothills: Onset of Mesozoic subduction in northern California: Journal of Geophysical Research, v. 114, no. B11, doi:10.1029/ 2009JB006607.
- EVARTS, R.C., 1977, The geology and petrology of the Del Puerto ophiolite, Diablo Range, central California Coast Ranges, *in* Coleman, R.G., and Irwin, W.P., eds., North American ophiolites: Oregon Department of Geology and Mineral Industries, Bulletin 95, p. 121–139.
- FRITZ, D.M., 1975, Ophiolite belt west of Paskenta, northern California Coast Range [MS Thesis]: Austin, Texas, University of Texas at Austin, 63 p.
- FULLER, C.W., WILLETT, S.D., AND BRANDON, M.T., 2006, Formation of forearc basins and their influence on subduction zone earthquakes, Geology, v. 34, p. 65–68, doi:10.1130/ G21828 1
- Gale, A.S., Mutterlose, J., and Batenburg, S., 2020, The Cretaceous Period, *in* Gradstein, F.M., Ogg, J.G., Schmitz, M.D., and Ogg, G.M., eds., Geologic Time Scale 2020: Amsterdam, Elsevier, p. 1023–1087.
- GARZANTI, E., 2016, From static to dynamic provenance analysis: sedimentary petrology upgraded: Sedimentary Geology, v. 336, p. 3–13.
- Garzanti, E., 2019, Petrographic classification of sand and sandstone: Earth-Science Reviews, v. 192, p. 545–563, doi:10.1016/j.earscirev.2018.12.014.
- GAZZI, P., 1966, Le arenarie del flysch sopracretaceo dell'Appennino modenese; correlazioni coni flysch di Monghidoro: Mineralogica et Petrographica Acta, v. 12, p. 69–97.
- Gehrels, G., 2012, Detrital zircon U-Pb geochronology: current methods and new opportunities, *in* Busby, C., and Azor, A., eds., Tectonics of Sedimentary Basins: Recent Advances: Chichester, John Wiley & Sons, p. 47–62, doi:10.1002/9781444347166.ch2.
- GEHRELS, G.E., AND PECHA, M., 2014, Detrital zircon U-Pb geochronology and Hf isotope geochemistry of Paleozoic and Triassic passive margin strata of western North America: Geosphere, v. 10, p. 49–65, doi:10.1130/GES00889.1.
- Gehrels, G.E., Valencia, V.A., and Ruiz, J., 2008, Enhanced precision, accuracy, efficiency, and spatial resolution of U-Pb ages by laser ablation–multicollector–inductively coupled plasma–mass spectrometry: Geochemistry Geophysics Geosystems, v. 9, no. Q03017, doi:10.1029/2007GC001805.
- GODFREY, N.J., BEAUDOIN, B.C., KLEMPERER, S.L., AND MENDOCINO WORKING GROUR, 1997, Ophiolitic basement to the Great Valley forearc basin, California, from seismic and gravity data: implications for crustal growth at the North American continental margin: Geological Society of America, Bulletin, v. 108, p. 1536–1562.
- GOUDKOFF, P.P., 1945, Stratigraphic relations of Upper Cretaceous in Great Valley, California: American Association of Petroleum Geologists, Bulletin, v. 29, p. 956–1007.
- Gradstein, F.M., Ogg, J.G., Schmitz, M.D., and Ogg, G.M., Geologic Time Scale 2020, Amsterdam, Elsevier.
- Graham, S.A., 1981, Stratigraphic and depositional patterns and hydrocarbon occurrence, Sacramento Valley, California, *in* Graham, S.A., ed., Field Guide to the Mesozoic–Cenozoic Convergent Margin of Northern California: American Association of Petroleum Geologists, Pacific Section, Book 50, p. 43–58.

- GREENE, T.J., AND SURPLESS, K.D., 2017, Facies architecture and provenance of a boulder-conglomerate submarine channel system, Panoche Formation, Great Valley Group: a forearc basin response to middle Cretaceous tectonism in the California convergent margin: Geosphere, v. 13, p. 838–869, doi:10.1130/GES01422.1.
- HACKEL, O., 1966, Summary of the geology of the Great Valley, in Bailey, E.H., ed., Geology of Northern California: California Division of Mines and Geology, Bulletin 190, p. 217–238.
- HACKER, B.R., DONATO, M.M., BARNES, C.G., McWILLIAMS, M.O., AND ERNST, W.G., 1995, Time scales of orogeny: Jurassic construction of the Klamath Mountains: Tectonics, v. 14, p. 677–703, doi:10.1029/94TC02454.
- HAEUSSLER, P.J., AND PATERSON S.R., 1993, Tilting, burial, and uplift of the Guadalupe igneous complex, Sierra Nevada, California: Geological Society of America, Bulletin, v. 105, p. 1310–1320, doi:10.1130/0016-7606(1993)105<1310:TBAUOT>2.3.CO;2.
- Hamilton, W., 1969, Mesozoic California and the underflow of Pacific mantle: Geological Society of America, Bulletin, v. 80, p. 2409–2430.
- HARPER, G.D., SALEEBY, J.B., AND HEIZLER, M., 1994, Formation and emplacement of the Josephine ophiolite and the Nevadan orogeny in the Klamath Mountains, California-Oregon: U/Pb zircon and ⁴⁰Ar/³⁹Ar geochronology: Journal of Geophysical Research, v. 99, p. 4293–4321, doi:10.1029/93JB02061.
- Heeszel, D.S., Wiens, D.A., Shore, P.J., Shiobara, H., and Sugioka, H., 2008, Earthquake evidence for along-arc extension in the Mariana Islands: Geochemistry, Geophysics, Geosystems, v. 9, p. 1–13, doi:10.1029/2008gc002186.
- Herriott, T.M., Crowley, J.L., Schmitz, M.D., Wartes, M.A., and Gillis, R.J., 2019, Exploring the law of detrital zircon: LA-ICP-MS and CA-TIMS geochronology of Jurassic forearc strata, Cook Inlet, Alaska, USA: Geology, v. 47, p. 1044–1048, doi:10. 1130/G46312.1.
- HOPSON, C.A., MATTINSON, J.M., AND PESSAGNO, E.A., Jr., 1981, Coast Range ophiolite, western California, in Ernst, W.G., ed., The Geotectonic Development of California: Englewood Cliffs, New Jersey, Prentice-Hall, p. 418–510.
- HOPSON, C.A., MATTINSON, J.M., PESSAGNO, E.A., Jr., AND LUYENDYK, B.P., 2008, California Coast Range ophiolite: composite Middle and Late Jurassic oceanic lithosphere, *in* Wright, J.E., and Shervais, J.W., eds., Ophiolites, Arcs, and Batholiths: A Tribute to Cliff Hopson: Geological Society of America, Special Paper 438, p. 1–101, doi: 10.1130/2008.2438(01).
- INGERSOLL, R.V., 1976, Evolution of the Late Cretaceous Forearc Basin of Northern and Central California [Ph.D. thesis]: Stanford, California, Stanford University, 200 p.
- INGERSOLL, R.V., 1978, Paleogeography and paleotectonics of the late Mesozoic fore-arc basin of northern and central California, in Howell, D.G., and McDougall, K.A., eds., Mesozoic Paleogeography of the Western United States: SEPM, Pacific Section, p. 471– 482
- INGERSOLL, R.V., 1979, Evolution of the Late Cretaceous forearc basin, northern and central California: Geological Society of America, Bulletin, v. 90, p. 813–826, doi:10.1130/0016-7606(1979)90<813:EOTLCF>2.0.CO;2.
- INGERSOLL, R.V., 1982, Initiation and evolution of the Great Valley forearc basin of northern and central California, U.S.A., in Leggett, J.K., ed., Trench–Forearc Geology: Sedimentation and Tectonics on Modern and Ancient Active Plate Margins: Geological Society of London, Special Publication 10, p. 459–467, doi:10.1144/GSL.SP.1982.010. 01.31.
- INGERSOLL, R.V., 1983, Petrofacies and provenance of late Mesozoic forearc basin: Northern and central California: American Association of Petroleum Geologists, Bulletin, v. 67, p. 1125–1142, doi:10.1306/03B5B713-16D1-11D7-8645000102C1865D.
- INGERSOLL, R.V., 1990, Nomenclature of upper Mesozoic strata of the Sacramento Valley of California: review and recommendations, in Ingersoll, R.V., and Nilsen, T.H., eds., Sacramento Valley Symposium and Guidebook: SEPM, Pacific Section, Book 65, p. 1–3.
- INGERSOLL, R.V., 2012, Tectonics of sedimentary basins, with revised nomenclature, in Busby, C., and Azor-Perez, A., eds., Tectonics of Sedimentary Basins: Recent Advances: Oxford, Blackwell, p. 3–43.
- INGERSOLL, R.V., 2019, Subduction-related sedimentary basins of the US Cordillera, in Miall, A.D., The Sedimentary Basins of the United States and Canada, Second Edition: Elsevier, p. 477–510, doi:10.1016/B978-0-444-63895-3.00011-5.
- INGERSOLL, R.V., RICH, E.I., AND DICKINSON, W.R., 1977, Great Valley Sequence, Sacramento Valley: Geological Society of America, Cordilleran Section, Field Guidebook, p. 1–72.
- INGERSOLL, R.V., BULLARD, T.F., FORD, R.L., GRIMM, J.P., PICKLE, J.D., AND SARES, S.W., 1984, The effect of grain size on detrital modes: a test of the Gazzi-Dickinson pointcounting method: Journal of Sedimentary Petrology, v. 54, p. 103–116.
- JAYKO, A.S., BLAKE, M.C., JR., AND HARMS, T.A., 1987, Attenuation of the Coast Range Ophiolite by extensional faulting, and nature of the Coast Range "thrust," California: Tectonics, v. 6, p. 475–488.
- Jones, D.L., 1975, Discovery of Buchia rugosa of Kimmeridgian age from the base of the Great Valley sequence [Abstract]: Geological Society of America, Abstracts with Programs, v. 7, p. 330.
- JONES, D.L., BAILEY, E.H., AND IMLAY, R.W., 1969, Structural and Stratigraphic Significance of the Buchia Zones in the Colyear Springs-Paskenta Area, California: U.S. Geological Survey, Professional Paper 647-A, 24 p.
- Kirby, J.M., 1943, Upper Cretaceous stratigraphy of west side of Sacramento Valley south of Willows, Glenn County, California: American Association of Petroleum Geologists, Bulletin, v. 27, p. 279–305.

- KNOPF, A., 1929, The Mother Lode system of California: U.S. Geological Survey, Professional Paper 157, 88 p., doi:10.3133/pp157.
- LAGABRIELLE, Y., ROURE, F., COUTELLE, A., MAURY, R.C., JORON, J.L., AND THONON, P., 1986, The Coast Range ophiolites (northern California): possible arc and back-arc basin remnants: their relations with the Nevadan orogeny: Société Géologique de France, Bulletin, v. 8, p. 981–999.
- Leary, R.J., Umhoefer, P., Smith, M.E., Smith, T.M., Saylor, J.E., Riggs, N., Burr, G., Lodes, E., Foley, D., Licht, A., Mueller, M.A., and Baird, C., 2020, Provenance of Pennsylvanian–Permian sedimentary rocks associated with the Ancestral Rocky Mountains orogeny in southwestern Laurentia: implications for continental-scale Laurentian sediment transport systems: Lithosphere, v. 12, p. 88–121, doi:10.1130/L1115.1.
- Lena, L., López-Martínez, R., Lescano, M., Aguire-Urreta, B., Concheyro, A., Vennari, V., Naipauer, M., Samankassou, E., Pimentel, M., Ramos, V.A., and Schaltegger, R., 2019, High-precision U—Pb ages in the early Tithonian to early Berriasian and implications for the numerical age of the Jurassic—Cretaceous boundary: Solid Earth, v. 10, p. 1–14, doi: 10.5194/se-10-1-2019.
- LINN, A.M., DEPAOLO, D.J., AND INGERSOLL, R.V., 1992, Nd-Sr isotopic, geochemical, and petrographic stratigraphy and paleotectonic analysis: Mesozoic Great Valley forearc sedimentary rocks of California: Geological Society of America, Bulletin, v. 104, p. 1264–1279.
- LOWE, D.R., 1979, Sediment gravity flows: their classification and some problems of application to natural flows and deposits, in Doyle, L.J., and Pilkey, O.H., eds., Geology of Continental Slopes: SEPM, Special Publication 27, p. 75–82.
- Lowe, D.R., 1982, Sediment gravity flows II. Depositional models with special reference to the deposits of high density turbidity currents: Journal of Sedimentary Petrology, v. 52, p. 279–297.
- MACDONALD, J.H., JR., HARPER, G.D., AND ZHU, B., 2006, Petrology, geochemistry, and provenance of the Galice Formation, Klamath Mountains, Oregon and California, in Snoke, A.W., and Barnes, C.G., eds., Geological Studies in the Klamath Mountains Province, California and Oregon: A Volume in Honor of William P. Irwin: Geological Society of America, Special Paper 410, p. 1–29, doi:10.1130/2006.2410(04).
- Maffione, M., van Hinsbergen, D.J.J., Koornneef, L.M.T., Guilmette, C., Hodges, K., Borneman, N., Huang, W., Ding, L., and Kapp, P., 2015, Forearc hyperextension dismembered the south Tibetan ophiolites: Geology, v. 43, p. 475–478, doi:10.1130/G36472.1
- Martin, M.W., and Clemens-Knott, D., 2015, Detrital-zircon record of the early Mesozoic southwestern Sierra Nevada are preserved in Lower Cretaceous intra-are and foreare deposits of central California, USA, *in* Anderson, T.H., Didenko, A.N., Johnson, C.L., Khanchuk, A.I., and MacDonald, J.H.Jr., eds., Late Jurassic Margin of Laurasia: A Record of Faulting Accommodating Plate Rotation: Geological Society of America, Special Paper 513, p. 269–284, doi:10.1130/2015.2513(06).
- MATTINSON, J.M., AND HOPSON, C.A., 1992, U/Pb ages of the Coast Range ophiolite: a critical reevaluation based on new high-precision Pb/Pb ages: American Association of Petroleum Geologists, Search and Discovery Article, #91016.
- McLaughlin, R.J., Blake, M.C., Jr., Griscom, A., Blome, C.D., and Murchey, B., 1988, Tectonics of formation, translation, and dispersal of the Coast Range ophiolite of California: Tectonics, v. 7, p. 1033–1056, doi:10.1029/TC007i005p01033.
- MIDDLETON, G.V., AND HAMPTON, M.A., 1973, Sediment gravity flows: mechanics of flow and deposition, in Middleton, G.V., and Bouma, A.H., eds., Turbidites and Deep-Water Sedimentation: SEPM, Pacific Section, Short Course Lecture Notes, p. 1–38.
- MITCHELL, C., GRAHAM, S.A., AND SUEK, D.H., 2010, Subduction complex uplift and exhumation and its influence on Maastrichtian forearc stratigraphy in the Great Valley Basin, northern San Joaquin Valley, California: Geological Society of America, Bulletin, v. 122, p. 2063–2078, doi:10.1130/B30180.1.
- MORRISON, R.R., BROWN, W.R., EDMONSON, W.F., THOMSON, J.N., AND YOUNG, R.J., 1971, Potential of Sacramento Valley gas province, California, *in* Cram, I.H., ed., Future Petroleum Provinces of the United States: Their Geology and Potential: American Association of Petroleum Geologists, Memoir 15, p. 329–338.
- MOXON, I.W., 1988, Sequence stratigraphy of the Great Valley basin in the context of convergent margin tectonics, in Graham, S.A., ed., Studies of the Geology of the San Joaquin Basin: SEPM, Pacific Section, Field Trip Guidebook 60, p. 3–28.
- MOXON, I.W., 1990, Stratigraphic and Structural Architecture of the San Joaquin– Sacramento Basin [Ph.D. Thesis]: Stanford, California, Stanford University, 371 p.
- MUTTI, E., 1992, Turbidite Sandstones: Istituto di Geologia Universita di Parma, Parma, Italy, 275 p.
- NODA, A., 2016, Forearc basins: types, geometries, and relationships to subduction zone dynamics: Geological Society of America, Bulletin, v. 128, p. 879–895, doi:10.1130/ B31345.1.
- Noda, A., and Miyakawa, A., 2016, Deposition and deformation of modern accretionary-type forearc basins *in* Itoh, Y., ed., Linking Basin Formation and Accretionary wedge growth: Evolutionary Models of Convergent Margins-Origin of Their Diversity: IntechOpen, doi:10.5772/67559.
- Ogg, J.G., AND HINNOY, L.A., 2012, Jurassic, *in* Gradstein, F.M., Ogg, J.G., Schmitz, M.D., and Ogg, G.M., eds., The Geologic Time Scale 2012, First Edition: Amsterdam, Elsevier, p. 731–791, doi:10.1016/B978-0-444-59425-9.00026-3.
- Ogg, J.G., Ogg, G.M., and Gradstein, F., 2016, A Concise Geologic Time Scale: Amsterdam, Elsevier.

- OJAKANGAS, R.W., 1968, Cretaceous sedimentation, Sacramento Valley, California: Geological Society of America, Bulletin, v. 79, p. 973–1008, doi:10.1130/0016-7606 (1968)791973:CSSVC12.0.CO;2.
- ORME, D.A., AND GRAHAM, S.A., 2018, Four-dimensional model of Cretaceous depositional geometry and sediment flux in the northern Great Valley forearc, California, in Ingersoll, R.V., Lawton, T.F., and Graham, S.A., eds., Tectonics, Sedimentary Basins, and Provenance: A Celebration of William R. Dickinson's Career: Geological Society of America, Special Paper 540, p. 409–424, doi:10.1130/2018.2540(18).
- Orme, D.A., and Surpless, K.D., 2019, The birth of a forearc: the basal Great Valley Group, California, USA: Geology, v. 47, p. 757–761, doi:10.1130/G46283.1.
- ORME, D.A., CARRAPA, B., AND KAPP, P., 2015, Sedimentology, provenance, and geochronology of the Upper Cretaceous–Lower Eocene western Xigaze forearc basin, southern Tibet: Basin Research, v. 27, p. 387–411, doi:10.1111/bre.12080.
- ORME, D.A., LASKOWSKI, A.K., ZILINSKY, M.F., CHAO, W., GUO, X., CAI, F., AND DING, L., 2021, Sedimentology and provenance of newly identified Upper Cretaceous trench-basin strata, Dênggar, southern Tibet: implications for development of the Eurasian margin prior to India–Asia collision: Basin Research, v. 33, p. 1454–1473, doi:10.1111/bre. 12521.
- PATERSON, S.R., AND MILLER, R.B., 1998, Magma emplacement during arc-perpendicular shortening: an example from the Cascades crystalline core, Washington: Tectonics, v. 17, p. 571–586, doi:10.1029/98TC01604.
- PATERSON, S.R., TOBISCH, O.T., AND VERNON, R.H., 1991, Emplacement and deformation of granitoids during volcanic arc construction in the Foothills terrane, central Sierra Nevada, California: Tectonophysics, v. 191, p. 89–110, doi:10.10116/0040-195(91) 90'34-1
- PESSAGNO, E.A., JR., 1977, Upper Jurassic Radiolaria and radiolarian biostratigraphy of the California Coast Ranges: Micropaleontology, v. 23, p. 56–113, doi:10.2307/1485310.
- Pullen, A., Ibáñez-Mejía, M., Gehrels, G.E., Ibáñez-Mejía, J.C., and Pecha, M., 2014, What happens when n = 1000? Creating large-n geochronological datasets with LA-ICP-MS for geologic investigations: Journal of Analytical Atomic Spectrometry, v. 29, p. 971–980, doi:10.1039/c4ja00023b.
- RATSCHBACHER, B.C., KELLER, C.B., SCHOENE, B., PATERSON, S.R., ANDERSON, J.L., OKAYA, D., PUTIRRA, K., AND LIPPOLDT, R., 2018, A new workflow to assess emplacement duration and melt residence time of compositionally diverse magmas emplaced in a subvolcanic reservoir: Journal of Petrology, v. 59, p. 1787–1809, doi:10.1093/petrology/egy079.
- REUTHER, C.D., AND ADAM, J., 1996, Forearc dynamics and neotectonic arc deformation, Central Andes, Northern Chile [Extended Abstract]: Third International Symposium on Andean Geodynamics, St. Malo, France, p. 219–222.
- RICCI-LUCCHI, F., 1975, Depositional cycles in two turbidite formations of northern Apennines (Italy): Journal of Sedimentary Petrology, v. 45, p. 3-43.
- ROBERTSON, A.H.F., 1990, Sedimentology and tectonic implications of ophiolite-derived clastics overlying the Jurassic Coast Range ophiolite, northern California: American Journal of Science, v. 290, p. 109–163.
- SALEEBY, J.B., 1982, Polygenetic ophiolite belt of the California Sierra Nevada: geochronological and tectonostratigraphic development: Journal of Geophysical Research, v. 87, p. 1803–1824.
- SALEEBY, J.B., 1992, Petrotectonic and paleogeographic settings of U.S. Cordilleran ophiolites, in Burchfiel, B.C., Lipman, P.W., and Zoback, M.L., eds., The Cordilleran Orogen: Conterminous U.S.: Geological Society of America, Geology of North America, v. G-3, p. 653–682.
- SALEEBY, J.B., AND BUSBY-SPERA, C., 1992, Early Mesozoic tectonic evolution of the western U.S. Cordillera, *in* Burchfiel, B.C., Lipman, P.W., and Zoback, M.L., eds., The Cordilleran Orogen: Conterminous U.S.: Geological Society of America, The Geology of North America, v. G-3, p. 107–138, doi:10.1130/DNAG-GNA-G3.107.
- SALEEBY, J.B., AND DUNNE, G., 2015, Temporal and tectonic relations of early Mesozoic arc magmatism, southern Sierra Nevada, California, in Anderson, T.H., Didenko, A.N., Johnson, C.L., Khanchuk, A.I., and MacDonald, J.H.Jr.., eds., Late Jurassic Margin of Laurasia: A Record of Faulting Accommodating Plate Rotation: Geological Society of America, Special Paper 513, p. 223–268, doi:10.1130/2015.2513(05).
- SALEEBY, J.B., GEARY, E.E., PATERSON, S.R., AND TOBISCH, O.T., 1989, Isotopic systematics of Pb/U (zircon) and ⁴⁰Ar/³⁹Ar (biotite-hornblende) from rocks of the central Foothills Terrane, Sierra Nevada, California: Geological Society of America, Bulletin, v. 101, p. 1481–1492.
- Schlüter, H.U., Gaedicke, C., Roeser, H.A., Schreckenberger, B., Meyer, H., Reichert, C., Diajadihardja, Y., and Prexl, A., 2002, Tectonic features of the southern Sumatrawestern Java forearc of Indonesia: Tectonics, v. 21, p. 111–1115, doi:10.1029/2001TC901048.
- SCHWARTZ, T.M., SCHWARTZ, R.K., AND WEISLOGEL, A.L., 2019, Orogenic recycling of detrital zircons characterizes age distributions of North American Cordilleran strata: Tectonics, v. 38, p. 4320–4334, doi:10.1029/2019TC005810.
- SCHWARTZ, T.M., SURPLESS, K.D., COLGAN, J.P., JOHNSTONE, S.A., AND HOLM-DENOMA, C.S., 2021, Detrital zircon record of magmatism and sediment dispersal across the North American Cordilleran arc system (28–48°N): Earth-Science Reviews, v. 220, no. 103734, doi:10.1016/i.earscirev.2021.103734.
- Schweickert, R.A., 2015, Jurassic evolution of the Western Sierra Nevada metamorphic province *in* Anderson, T.H., Didenko, Johnson, C.L., Khanchuk, A.I., and MacDonald, J.H., Jr., eds., Late Jurassic Margin of Laurasia: A Record of Faulting Accommodating

- Plate Rotation: Geological Society of America, Special Paper 513, p. 299–358, doi:10. 1130/2015.2513(08).
- SCHWEICKERT, R.A., BOGEN, N.L., GIRTY, G.H., HANSON, R.E., AND MERGUERIAN, C., 1984, Timing and structural expression of the Nevadan orogeny, Sierra Nevada, California: Geological Society of America, Bulletin, v. 95, p. 967–979.
- SCHWEICKERT, R.A., AND COWAN, D.S., 1975, Early Mesozoic tectonic evolution of the western Sierra Nevada, California: Geological Society of America, Bulletin, v. 86, p. 1329–1336.
- SEIDERS, V.M., AND BLOME, C.D., 1988, Implications of upper Mesozoic conglomerate for suspect terrane in western California and adjacent areas: Geological Society of America, Bulletin, v. 100, p. 374–391.
- Seton, M., Müller, R.D., Zahirovic, S., Gaina, C., Torsvik, T., Shephard, G., and Chandler, M., 2012, Global continental and ocean basin reconstructions since 200 Ma: Earth-Science Reviews, v. 113, p. 212–270.
- SHARMAN, G.R., GRAHAM, S.A., GROVE, M., KIMBROUGH, D.L., AND WRIGHT, J.E., 2015, Detrital zircon provenance of the Late Cretaceous–Eocene California forearc: influence of Laramide low-angle subduction on sediment dispersal and paleogeography: Geological Society of America, Bulletin, v. 127, p. 38–60, doi:10.1130/B31065.1.
- SHARMAN, G.R., SHARMAN, J.P., AND SYLVESTER, Z., 2018, detritalPy: a Python-based toolset for visualizing and analysing detrital geo-thermochronologic data: The Depositional Record, v. 4, p. 202–215, doi:10.1002/dep2.45.
- SHERVAIS, J.W., 2001, Birth, death and resurrection: the life cycle of suprasubduction zone ophiolites: Geochemistry, Geophysics, Geosystems, v. 2, no. 1010, doi:10.1029/ 2000GC000080.
- SHERVAIS, J.W., MURCHEY, B.L., KIMBROUGH, D.L., RENNE, P.R., AND HANAN, B., 2005, Radioisotopic and biostratigraphic age relations in the Coast Range Ophiolite, northern California: implications for the tectonic evolution of the Western Cordillera: Geological Society of America, Bulletin, v. 117, p. 633–653, doi:10.1130/B25443.1.
- SHORT, P.F., AND INGERSOLL, R.V., 1990, Petrofacies and provenance of the Great Valley Group, southern Klamath Mountains and northern Sacramento Valley, *in* Ingersoll, R.V., and Nilsen, T.H., eds., Sacramento Valley Symposium and Guidebook: SEPM, Pacific Section, Book 65, p. 39–52.
- SHULTZ, A., 1984, Subaerial debris-flow deposition in the upper Paleozoic Cutler Formation, western Colorado: Journal of Sedimentary Petrology, v. 54, p. 759–772.
- SNOW, C.A., AND ERNST, W.G., 2008, Detrital zircon constraints on sediment distribution and provenance of the Mariposa Formation, central Sierra Nevada foothills, California, in Wright, J.E., and Shervais, J.W., eds., Ophiolites, Arcs, and Batholiths: A Tribute to Cliff Hopson: Geological Society of America, Special Paper 435, p. 311–330.
- STERN, T.W., BATEMAN, P.C., MORGAN, B.A., NEWELL, M.F., AND PECK, D.L., 1981, Isotopic U-Pb ages of zircon from the granitoids of the central Sierra Nevada, California: U.S. Geological Survey, Professional Paper 1185, 17 p., doi:10.2133/pp1185.
- SUCHECKI, R.K., 1984, Facies history of the Upper Jurassic-Lower Cretaceous Great Valley Sequence: response to structural development of an outer-arc basin: Journal of Sedimentary Petrology, v. 54, p. 170–191.
- SUNDELL, K.E., GEHRELS, G.E., BLUM, M.D., SAYLOR, J.E., PECHA, M.E., AND HUNDLEY, B.P., 2024, An exploratory study of "large-n" detrital zircon geochronology of the Book Cliffs, UT via rapid (3s/analysis) U-Pb dating: Basin Research, v. 36, no. e12840. doi:10.1111/bre.12840.
- SURPLESS, K.D., 2014, Geochemistry of the Great Valley Group: an integrated provenance record: International Geology Review, v. 57, p. 747–766, doi:10.1080/00206814.2014. 923347.
- Surpless, K.D., and Augsburger, G.A., 2009, Provenance of the Pythian Cave conglomerate, northern California: implications for mid-Cretaceous paleogeography of the U.S. Cordillera: Cretaceous Research, v. 30, p. 1181–1192, doi:10.1016/j.cretres. 2009.05.005.
- Surpless, K.D., Graham, S.A., Covault, J.A., and Wooden, J.L., 2006, Does the Great Valley Group contain Jurassic strata? Reevaluation of the age and early evolution of a classic forearc basin: Geology, v. 34, p. 21–24, doi:10.1130/G21940.1.
- Surpless, K.D., Clemens-Knott, D., Barth, A.P., and Gevedon, M., 2019, A survey of Sierra Nevada magmatism using Great Valley detrital zircon trace-element geochemistry: view from the foreare: Lithosphere, v. 11, p. 603–619, doi:10.1130/L1059.1.
- Surpless, K.D., Alford, R.W., Barnes, C., Yoshinobu, A., and Weis, N., 2023, Late Jurassic paleogeography of the US Cordillera from detrital zircon age and hafnium

- analysis of the Galice Formation, Klamath Mountains, Oregon and California, USA: Geological Society of America, Bulletin, v. 136, p. 1488–1510, doi:10.1130/B36810.1.
- Tobisch, O.T., Fiske, R.S., Saleeby, J.B., Holt, E., and Sorensen, S.S., 2000, Steep tilting of metavolcanic rocks by multiple mechanisms, central Sierra Nevada, California: Geological Society of America Bulletin, v. 112, p. 1043–1058, doi:10.1130/0016-7606 (2000)112 <1043:STOMRB>2.0 CO;2.
- VERMEESCH, P., 2013, Multi-sample comparison of detrital age distributions: Chemical Geology, v. 341, p. 140–146, doi:10.1016/j.chemgeo.2013.01.010.
- Vermeesch, P., 2018, IsoplotR: a free and open toolbox for geochronology: Geoscience Frontiers, v. 9, p. 1479–1493, doi:10.1016.j.gsf.2018.04.001.
- Vermeesch, P., 2021, Maximum depositional age estimation revisited: Geoscience Frontiers, v. 12, p. 843–850, doi:10.1016/j.gsf.2020.08.008.
- VOGEL, K.D., 1985, Deformation in the lower Great Valley sequence: the Paskenta fault zone of northern California [M.A. Thesis]: Austin, University of Texas, 129 p.
- VOGEL, K.D., AND CLOOS, M., 1985, Deformation in the lower Great Valley sequence: the Paskenta fault zone of northern California [Abstract]: Geological Society of America, Abstracts with Programs, v. 17, p. 415.
- WAKABAYASHI, J., 2011, Mélanges of the Franciscan Complex, California: diverse structural settings, evidence for sedimentary mixing, and their connection to subduction processes, in Wakabayashi, J., and Dilek, Y., eds., Mélanges: Processes of Formation and Societal Significance: Geological Society of America, Special Paper 480, p. 117–141, doi:10. 1130/2011.2480(05).
- WAKABAYASHI, J., 2019, Sedimentary compared to tectonically-deformed serpentinites and tectonic serpentinites and tectonic serpentinite mélanges at outcrop to petrographic scales: unambiguous and disputed examples from California: Gondwana Research, v. 74, p. 51-67, doi:10.1016/j.gr.2019.04.005.
- WALKER, R.G., 1965, The origin and significance of the internal sedimentary structures of turbidites: Yorkshire Geological Society, Proceedings, v. 35, p. 1–32.
- WALKER, R.G., 1975, Generalized facies models for the resedimented conglomerates of turbidite association: Geological Society of America, Bulletin, v. 86, p. 737–748.
- WALKER, R.G., AND MUTTI, E., 1973, Turbidite facies and facies associations, in Middleton, G.V., and Bouma, A.H., eds., Turbidites and Deep Water Sedimentation: SEPM, Pacific Section, Short Course, p. 119–158.
- WILLETT, S.D., AND SCHUNEGGER, F., 2010, The last phase of deposition in the Swiss Molasse Basin: from foredeep to negative-alpha basin: Basin Research, v. 22, p. 623–639, doi:10.1111/j.1365-2117.2009.00435.x.
- WILLIAMS, T.A., 1997, Basin-Fill Architecture and Forearc Tectonics: Cretaceous Great Valley Group, Sacramento Basin, Northern California [Ph.D. Thesis]: Stanford, California, Stanford University, 412 p.
- WILLIAMS, T.A., AND GRAHAM, S.A., 2013, Controls on forearc basin architecture from seismic and sequence stratigraphy of the Upper Cretaceous Great Valley Group, central Sacramento Basin, California: International Geology Review, v. 55, p. 2030–2059, doi:10.1080/00206814.2013.817520.
- WIMBLEDON, W.A.P., REHAKOVA, D., SVOBODOVA, A., ELBRA, T., SCHNABL, P., PRUNER, P., SIFNEROVA, K., KDYR, S., DZYUBA, O.S., SCHNYDER, J., GALBRUN, B., KOSTAK, M., VANKOVA, L., COPESTAKE, P., HUNT, C., RICCARDI, A., POULTON, T.P., BULOT, L.G., FRAU, C., AND DE LENA, L., 2020, The proposal of a GSSP for the Berriasian Stage (Cretaceous System): Part 1: Volumina Jurassica, v. 18, p. 53–106, doi:10.7306/vj.18.5.
- WRIGHT, J.E., AND WYLD, S.J., 2007, Alternative tectonic model for Late Jurassic through Early Cretaceous evolution of the Great Valley Group, California, in Cloos, M., Carlson, W.D., Gilbert, M.C., Liou, J.G., and Sorenson, S.S., eds., Convergent Margin Terranes and Associated Regions: A Tribute to W.G. Ernst: Geological Society of America, Special Paper 419, p. 81–95, doi:10.1130/2007.2419(04).
- ZAKHAROV, V.A., AND ROGOV, M.A., 2020, High-resolution stratigraphy of buchiid bivalves and ammonites from the Jurassic-Cretaceous boundary beds in the Paskenta area (California): Cretaceous Research, v. 110, no. 104422, doi:10.1016/j.cretres.2020. 104422.

Received 4 January 2024; accepted 29 July 2024.